1 Plateaus and jumps in the atmospheric radiocarbon record – Potential origin and value

2 as global age markers for glacial-to-deglacial paleoceanography, a synthesis

5 Michael Sarnthein[1], Kevin Küssner[2], Pieter M. Grootes[3], Blanca Ausin[4][8], Timothy

6 Eglinton[8], Juan Muglia[5], Raimund Muscheler[6], Gordon Schlolaut[7]

9 1) Institute of Geosciences, University of Kiel, Olshausenstr. 40, 24098 Kiel, Germany,

10 michael.sarnthein@ifg.uni-kiel.de, (corresponding author)

11 2) Alfred-Wegener-Institut Helmholtz-Zentrum für Polar- und Meeresforschung,

12 Department for Marine Geology, 27570 Bremerhaven, Germany, kevin.kuessner@awi.de

13 3) Institute of Ecosystem Research, University of Kiel, Olshausenstr. 40, 24098 Kiel,

14 Germany, pgrootes@ecology.uni-kiel.de

15 4) Geology Department, University of Salamanca, Plaza de los Caldos, 37008

16 Salamanca, Spain, <ausin@usal.es>

17 5) Centro para el Estudio de los Sistemas Marinos, CONICET, 2915 Boulevard Brown,

18 U9120ACD, Puerto Madryn, Argentina, jmuglia@cenpat-conicet.gob.ar

19 6) Quaternary Sciences, Department of Geology Lund University, Sölvegatan 12, 22362

20 Lund, Sweden, raimund.muscheler@geol.lu.se

21 7) Climate Dynamics and Landscape Evolution, GFZ German Centre for Geosciences,

22 Telegrafenberg, 14473 Potsdam, Germany, SchlolautG@gmail.com

23 8) Geological Institute, ETH Zürich, Sonneggstr. 5, 8092 Zuerich, Switzerland,

26 final version submitted to CLIMATE OF THE PAST (2020-08-8)

29   ABSTRACT

30   Changes in the geometry of ocean Meridional Overturning Circulation (MOC) are crucial in

31   controlling past changes of climate and the carbon inventory of the atmosphere. However, the

32   accurate timing and global correlation of short-term glacial-to-deglacial changes of MOC in

33   different ocean basins still present a major challenge. The fine structure of jumps and plateaus

34   in atmospheric and planktic radiocarbon (^{14}C) concentration reflects changes in atmospheric ^{14}C

35   production, ocean-atmosphere ^{14}C exchange, and ocean mixing. Plateau boundaries in the

36   atmospheric ^{14}C record of Lake Suigetsu, now tied to Hulu U/Th model-ages instead of optical

37   varve counts, provide a stratigraphic 'rung ladder' of up to 30 age tie points 29 to 10 cal. ka for

38   accurate dating of planktic oceanic ^{14}C records. The age differences between contemporary

39   planktic and atmospheric ^{14}C plateaus record the global distribution of ^{14}C reservoir ages for

40   surface waters of the Last Glacial Maximum (LGM) / deglacial Heinrich Stadial 1 (HS-1), as

41   documented in 19/20 planktic ^{14}C records. Elevated and variable reservoir ages mark both

42   upwelling regions and high-latitude sites covered by sea ice and/or meltwater. ^{14}C ventilation

43   ages of LGM deep waters reveal opposed geometries of Atlantic and Pacific MOC. Like today,

44   Atlantic deep-water formation went along with an estuarine inflow of old abyssal waters from the

45   Southern Ocean up to the northern North Pacific and an outflow of upper deep waters. During

46   early HS-1, ^{14}C ventilation ages suggest a reversed MOC and ~1500 year-long flushing of the

47   deep North Pacific up to the South China Sea, when estuarine circulation geometry marked the

48   North Atlantic, gradually starting near 19 ka. High ^{14}C ventilation ages of LGM deep waters

49   reflect a major drawdown of carbon from the atmosphere. The subsequent major deglacial age

50   drop reflects changes in MOC accompanied by massive carbon releases to the atmosphere as

51   recorded in Antarctic ice cores. These new features of MOC and the carbon cycle provide

52   detailed evidence in space and time to test and refine ocean models that, in part because of

53   insufficient spatial model resolution and reference data, still poorly reproduce our data sets.

1. INTRODUCTION

1.1 A variety of terms linked to the notion '^{14}C age'

The ^{14}C concentration in the troposphere is mainly determined by ^{14}C production, atmospheric mixing, moreover, air-sea gas exchange and ocean circulation that vary over time (e.g., Alves et al., 2018; Alveson et al., 2018). The ^{14}C content of living terrestrial plants is in equilibrium with the atmosphere via processes of photosynthesis and respiration. Accordingly, the ^{14}C of terrestrial plant remains in a sediment section directly reflects the amount of radioactive decay, thus the time passed since the plant's death, and the ^{14}C composition of the atmosphere during the time of plant growth.

Contrariwise, ^{14}C values of marine and inland waters are cut off from cosmogenic ^{14}C production in the atmosphere, hence depend on the carbon transfer at the air-water interface and the result of local transport and mixing of carbon in the water. For surface waters, the air-sea transfer involves a time span of ten years and less (e.g., Nydal et al., 1998). Yet, vertical and horizontal water mixing results in surface ocean ^{14}C concentrations on average 5 % lower than those in the contemporaneous atmosphere, a difference expressed as 'Marine Reservoir Age' (or 'reservoir effect' *sensu* Alves et al., 2018). These 'ages' reflect the local oceanography and are highly variable through time (~200–2500 yr; e.g., Stuiver and Braziunas, 1993; Grootes and Sarnthein, 2006; Sarnthein et al., 2015). Apart from U/Th dated corals (many papers on their reservoir age since Adkins and Boyle, 1997), the ^{14}C age of planktic foraminifers is the most common tracer in marine sediments providing a rough estimate of the time passed since sediment deposition. Soon, however, marine geologists were confronted with age inconsistencies that implied a series of unknowns, in particular the surface ocean ^{14}C 'reservoir age' that finally became a most valuable tracer for oceanography.

81

82 The ^{14}C records of benthic foraminifers in deep-sea sediments reflect the time of

83 radioactive decay since their deposition with the apparent 'ventilation age' of the deep

84 waters in which they lived. Ventilation age is primarily the time span from the moment

85 when carbon dissolved in the local surface waters with somewhat reduced ^{14}C level lost

86 contact with the atmosphere until the precipitation of benthic carbonate from the down-

87 welled deep waters. Details on the derivation of ventilation ages are provided in Cook

88 and Keigwin (2015) and Balmer and Sarnthein (2018). In addition, however, ventilation

89 ages include hardly quantifiable lateral admixtures of older and/or younger water

90 masses, moreover, ^{14}C-enriched organic carbon supplied by the biological pump, thus

91 are called 'apparent'. Today, the apparent transit times of carbon dissolved in the deep

92 ocean range from a few hundred up to ~1800 ^{14}C yr found in upper deep waters of the

93 northeastern North Pacific (Matsumoto, 2007).

94

95 The reservoir ages of surface waters and the ventilation ages of deep waters present

96 robust and high-resolution tracers essential for drawing quantitative conclusions on past

97 ocean circulation geometries, marine climate change, and the processes that drive both

98 past ocean dynamics and carbon budgets, given the ages rely on a number of robust

99 age tie points. Obtaining such tie points presents a problem, since any attempt to date a

100 deep-sea sediment record by means of ^{14}C encounters a number of intricacies of how to

101 disentangle the effects of global atmospheric ^{14}C variations due to past changes in

102 cosmogenic ^{14}C production and carbon cycle from (i) local depositional effects such as

103 sediment hiatuses and winnowing, differential bioturbational mixing depth, and sediment

104 transport by deep burrows, (ii) the effects of local atmosphere-ocean exchange and

105 ocean mixing resulting in reservoir and ventilation ages that change through time and

106   space (e.g., Alves et al. 2018; Grootes and Sarnthein, 2006), and (iii) from the final

107   target, quantitatively 'pure' ^{14}C ages due to radioactive decay. These problems are

108   exacerbated by the need for a generally accepted high-precision atmospheric reference

109   record for the period 14–50 cal. ka, beyond tree ring calibration,

110

111   Current ^{14}C-based chronologies of deep-sea sediment records, used to constrain and

112   correlate the age of glacial-to-deglacial changes in ocean dynamics and climate on a

113   global scale, are often of insufficient quality when they are based on (i) age tie points

114   spaced far too wide (e.g., using DO-events 1, 2, and 3 only and/or sporadic tephra

115   layers for the time span 30–14 cal ka), (ii) disregarding atmospheric ^{14}C plateaus, (iii)

116   the risky assumption of ±constant planktic ^{14}C reservoir ages and other speculative

117   stratigraphic correlations/compilations, and (iv) ignoring small-scale major differences in

118   low-latitude reservoir age. Likewise, clear conclusions are precluded by an uncertainty

119   range of 3-4 kyr sometimes accepted for tie points during the glacial-to-deglacial period

120   (Stern and Lisiecki, 2013; Lisiecki and Stern, 2016), where significant global climate

121   oscillations occurred on decadal-to-centennial time scales as widely shown on the basis

122   of speleothem and ice core-based records (Steffensen et al., 2008; Svensson et al.,

123   2008; Wang et al., 2001). Thus marine paleoclimate and paleoceanographic studies

124   today focus on the continuing quest for a high-resolution and global, hence necessarily

125   atmospheric ^{14}C reference record.

126

127   *1.2 Review of tie points used to fix calibrated and reservoir ages in marine ^{14}C records*

128   The tree ring-based calibration of ^{14}C ages provides a master record of decadal

129   changes in atmospheric ^{14}C concentrations back to ~14 cal. ka (Reimer et al., 2013 and

130   2020) with floating sections beyond (from ~12.5–14.5 cal. ka, around 29–31.5 and 43

131   cal. ka; Turney et al., 2010, 2017, Reimer et al., 2020). The evolution of Holocene and

132   late deglacial ^{14}C ages with time is not linear but reveals variations with numerous

133   distinct jumps (= rapid change) and (short) plateau-shaped (slow or no change or even

134   inversion) structures indicative of fluctuations in atmospheric ^{14}C concentration. Prior to

135   8500 cal. yr BP, various plateaus extend over 400–600 cal. yr and beyond (Fig. 2).

136   Given the quality of the tree ring calibration data, these fluctuations can be considered

137   real, suitable for global correlation (Sarnthein et al., 2007, 2015; Umling and Thunnell,

138   2017; Sarnthein and Werner, 2018). Air-sea gas exchange transfers the atmospheric

139   ^{14}C fluctuations into the surface ocean where they can provide high-resolution tie points

140   to calibrate the marine ^{14}C record and marine reservoir ages back to ~14 ka (via "^{14}C

141   wiggle matching"). In the near future, however, it is unlikely that a continuous tree ring-

142   based record will become available to trace such atmospheric ^{14}C variations further

143   back, over the period 14–29 cal. ka crucial for the understanding of last-glacial-to-

144   interglacial changes in climate. Hence various other, carbonate-based ^{14}C archives

145   have been employed for this period to reconstruct past changes in atmospheric ^{14}C

146   concentration/age and tie them to an 'absolute' or 'calibrated' (e.g., incremental and/or

147   based on speleothem carbonate) age scale.

148

149   Suites of ^{14}C ages of paired marine and terrestrial plant-borne samples, e.g. paired

150   planktic foraminifers and wood chunks, provide most effective but rarely realizable

151   absolute-age markers and reservoir ages of local ocean surface waters (Zhao and

152   Keigwin, 2018; Rafter et al., 2018; Schroeder et al., 2016; Broecker et al., 2004).

153   Likewise successful appears the alignment of ^{14}C-dated variations in downcore sea-

154   surface temperatures (SST) with changes in hydroclimate as recorded in age-calibrated

155   sedimentary leaf-wax hydrogen isotope (δD) records from ancient lakes (Muschitiello et

156 al., 2019), assumed to be coeval. Further tie points are derived from volcanic ash layers

157 (Waelbroeck et al., 2001; Siani et al, 2013; Davies et al., 2014; Sikes and Guilderson,

158 2016), paired U/Th- and ^{14}C-based coral ages (Adkins and Boyle, 1997; Robinson et al.,

159 2005; Burke and Robinson, 2012; Chen et al., 2015), and the (fairly fragmentary)

160 alignment of major tipping points in ^{14}C dated records of marine SST and planktic δ^{18}O

161 to the incremental age scale of climate events dated in polar ice core records

162 (Waelbroeck et al., 2011). Such well-defined tie points, however, are wide-spaced in

163 peak glacial-to-early deglacial ice core records, too wide for properly resolving a clear

164 picture of the spatiotemporal pattern of marine paleoclimate events. Finally, various

165 data compilations tentatively rely on the use of multiple age correlations amongst

166 likewise poorly dated marine sediment records, an effort necessarily problematic.

167 Skinner et al. (2019) recently combined new and existing reservoir age estimates from

168 North Atlantic and Southern Ocean to show coherent but distinct regional reservoir age

169 trends in subpolar ocean regions, trends that indeed envelop the range of actual major

170 small-scale and short-term oscillations in reservoir age revealed by our technique of ^{14}C

171 plateau tuning for the subpolar South Pacific (Küssner et al., 2020 subm.).

172

173 Lacking robust age tie points several authors resort to ^{14}C reservoir age simulations for

174 various sea regions by ocean General Circulation Models (GCM) (e.g. Butzin et al.,

175 2017; Muglia et al., 2018) to quantify the potential difference between marine and

176 atmospheric ^{14}C dates for glacial-to-interglacial times. In view of the complexity of ocean

177 MOC and the global carbon cycle it is not surprising that the results of a comparison of

178 a selection of robust empiric vs. simulated ^{14}C reservoir ages are not that encouraging

179 yet (as discussed further below).

180

181   Beyond accepting a generally close link between ^{14}C concentrations in the troposphere

182   and in the surface ocean, the fine structure of planktic ^{14}C records with centennial-scale-

183   resolution can provide a far superior (though costly) link of the marine sediment records

184   to the reference suite of narrow-standing jumps and boundaries of the plateaus robustly

185   identified in the atmospheric ^{14}C record of Lake Suigetsu, the only long, continuous

186   record based on terrestrial plant remains (Bronk Ramsey et al., 2012, 2019). Beyond

187   the reach of the tree ring-based age scale ~14 cal. ka, the absolute age of the Suigetsu

188   atmospheric ^{14}C structures can be either calibrated by incremental (microscopy- or

189   XRF-based) varve counts (Schlolaut et al., 2018; Marshall et al., 2012) or by a series of

190   paired U/Th- and ^{14}C-based model ages correlated from the Hulu Cave speleothem

191   record (Bronk Ramsey, 2012 and 2019; Southon et al., 2012; Cheng et al., 2018). The

192   difference in absolute age between these calibrations (Fig. 3) is of little importance for

193   the tuning of planktic to corresponding atmospheric ^{14}C plateaus and the derivation of

194   planktic reservoir ages that present the highly variable offset of the ^{14}C age of a planktic

195   plateau from that of the correlated atmospheric plateau. The offset is deduced by

196   subtracting the average ^{14}C age of an atmospheric ^{14}C plateau from that of the

197   correlated planktic ^{14}C plateau, independent of any absolute age value assigned.

198

199   The uncertainty of the Suigetsu atmospheric 14C record is significantly larger than that

200   of the tree ring-based calibration record because of lower 14C concentrations, limited

201   sampling density, and uncertainties in the independent age determination. Thus the ^{14}C

202   fluctuations could be real or represent mere statistical scatter (null hypothesis) in which

203   case the record of atmospheric ^{14}C ages against time would show a simple continuous

204   rise resulting from radioactive decay and the advance of time, such as suggested by a

205 fairly straight progression of the highly resolved deglacial Hulu Cave ^{14}C record plotted

206 vs. U/Th ages (Southon et al., 2012; Cheng et al., 2018).

207

208 The unequivocal fluctuations in the tree ring-based master record of atmospheric ^{14}C

209 concentration (Fig. 2; Reimer et al., 2013, 2020) are on the order of 2–3 % over the last

210 10 kyr (Stuiver and Braziunas, 1993) and even larger back to ~14 ka. Under glacial and

211 deglacial low-CO_2 conditions beyond 14 ka, when climate and ocean dynamics were

212 less constant than during the Holocene, real atmospheric ^{14}C fluctuations were, most

213 likely, even stronger and ^{14}C plateaus and jumps accordingly larger. Plateau-jump

214 structures are also becoming increasingly evident in the evolving atmospheric

215 calibration record (Reimer et al., 2020). The age-defined plateaus and jumps in the

216 Suigetsu atmospheric ^{14}C calibration curve may thus be regarded as a suite of 'real'

217 structures, extending the calibration provided by the tree ring record for Holocene and

218 B/A-to-Early Holocene times (Fig. 2) into early deglacial and LGM times.

219

220 The plateau/jump structures may partly be linked to changes in cosmogenic ^{14}C

221 production, as possibly shown in the ^{10}Be record (Fig. 4; based on data of Adolphi et al.,

222 2018), and – presumably more dominant – to short-term changes in ocean mixing and

223 the carbon exchange between ocean and atmosphere. The exchange is crucial, since

224 the carbon reservoir of the ocean contains up to 60 (preindustrial) atmospheric carbon

225 units (Berger and Keir, 1984). The apparent contradiction with the smooth Hulu Cave

226 ^{14}C record (Southon et al., 2012; Cheng et al., 2018) may possibly be explained by the

227 Hulu Cave speleothem precipitation system acting as a low-pass filter for fluctuating

228 atmospheric ^{14}C concentrations (statistical tests of Bronk Ramsey et al., 2020) and, to a

229 very limited degree, by the obvious scatter in the Suigetsu data. The filter for Hulu data

230 possibly led to a loss especially of short-lived structures in the preserved atmospheric

231 ^{14}C record, though some remainders were preserved in the ^{14}C records of Hulu Cave

232 (Fig. 1). So we rather trust the amplitude of Suigetsu ^{14}C structures than the timing of

233 Hulu Cave data.

234

235 Like a 'rung ladder' the age-calibrated suite of ^{14}C plateau boundaries and jumps is

236 suited for tracing the calibrated age of numerous plateau boundaries in glacial-to-

237 deglacial marine ^{14}C records likewise densely sampled, even when some rungs have

238 been destroyed by local influences on gas exchange or ocean mixing. Also, one may

239 record the average offset of planktic ^{14}C ages from paired atmospheric ^{14}C ages, i.e. the

240 planktic reservoir age, for each single ^{14}C plateau (Sarnthein et al., 2007, 2015). We

241 prefer the Suigetsu record to IntCal, since it is based on original primary atmospheric

242 data and results in small-scale spatio-temporal changes of reservoir age, whereas

243 IntCal is mixing and smoothing a broad array of different data sources with comparativ-

244 ely coarse age resolution, including carbonate-based speleothem and marine records.

245 For the first time, this suite of tie points may facilitate a precise temporal correlation of

246 all sorts of changes in surface and deep-water composition on a global scale, crucial for

247 a better understanding of past changes in ocean and climate dynamics.

248

249 *1.3 Items discussed in this synthesis*

250 The Results Section is summarizing (1) Means to separate noise, global atmospheric

251 and local oceanic forcings that together control the structure of a planktic ^{14}C plateaus,

252 (2) The choice of a U/Th-based reference time scale (Bronk Ramsey et al. 2012; Cheng

253 et al., 2018) instead of the earlier varve-counted version (Schlolaut et al., 2018) to date

254 the structures in the global atmospheric ^{14}C record of Lake Suigetsu (Sarnthein et al.,

255 2015), (3) The extension of the suite of age tie points from 23 back to 29 cal. ka, values

256 crucial for an accurate global correlation of ocean events over the Last Glacial

257 Maximum, and (4) Potential linkages of atmospheric ^{14}C plateaus and jumps to

258 cosmogenic ^{14}C production and/or ocean dynamics.

259

260 The Discussion and Implications section includes:

261 (1) A global summary of published marine ^{14}C reservoir age records (Sarnthein et al.

262 2015) now enlarged by nine plateau-tuned records from the Southern Hemisphere

263 (Balmer et al., 2016 and 2018; Küssner et al., 2018 and 2020 subm.) and the northeast

264 Atlantic (Ausin et al., 2020 subm.). In total, 18 (LGM) / 19 (HS-1) plus three wood

265 chunk-based records (Broecker et al., 2004; Zhao et al., 2018) now depict the spatio-

266 temporal variability of past reservoir ages of surface waters in different ocean regions.

267 (2) A comparison of our plateau-based reservoir ages with LGM estimates of surface

268 water ^{14}C reservoir ages simulated by the GCM of Muglia et al. (2018).

269 (3) More detailed insights into the origin of past changes in the global carbon cycle from

270 glacial to interglacial times are provided by the enlarged set of ^{14}C reservoir and venti-

271 lation ages that form a robust tracer of global circulation geometries and the inorganic

272 carbon (DIC) dissolved in different basins of the ocean (Sarnthein et al., 2013).

273

274 The discussion highlights ^{14}C plateau tuning and its revised cal. time scale for global

275 data-model intercomparison and a new understanding of Ocean MOC during the LGM

276 and its reversal during HS-1.

277

278 2. RESULTS – AGE TIE POINTS BASED ON ^{14}C PLATEAU BOUNDARIES

279

280   2.1 *Suite of planktic ^{14}C plateaus: Means to separate global atmospheric from local*

281   *oceanographic forcings*

282   The basic assumption of the ^{14}C plateau tuning technique is that the fine structure of

283   fluctuations of the global atmospheric ^{14}C concentration record can also be found in the

284   surface ocean. In a plot of ^{14}C age versus calendar age such fluctuations lead to a pattern

285   of plateaus/jumps that correspond to decreases/increases in ^{14}C concentration. Here we

286   refer to the derivation and interpretation of planktic ^{14}C plateaus, assuming a predom-

287   inantly global atmospheric origin with occasional local oceanographic forcings. The series

288   of planktic ^{14}C plateaus and jumps are derived in cores with average hemipelagic

289   sedimentation rates of >10 cm/ky and dating resolution of <100-150 yr. The plateau-

290   specific structures in a sediment age-depth record form a well-defined suite for which

291   absolute age and reservoir age are derived by means of a strict alignment to the reference

292   suite of global atmospheric ^{14}C plateaus as a whole. Initially, age tie points of planktic

293   foraminiferal δ^{18}O records showing (orbital) isotope stages #1-3 serve as stratigraphic

294   guideline for the alignment under the simplifying assumption that stratigraphic gaps are

295   absent, not always true (Suppl. Fig. 2). Planktic reservoir ages and their short-term

296   changes are derived from the difference in average ^{14}C age between atmosphere and

297   surface waters in subsequent plateaus. To stick as close as possible to the modern range

298   of reservoir ages (Stuiver and Braziunas, 1993), tuned reservoir ages are kept at a

299   minimum unless stringent evidence requires otherwise.

300

301   A close correspondence between ^{14}C concentrations in atmosphere and surface ocean

302   is expected based on rapid gas exchange. In several cases, however, the specific

303   structure and relative length of a planktic ^{14}C plateau may deviate from those of the

304   pertinent plateau observed within the suite of atmospheric plateaus, thus indicate local

305   intra-plateau changes of reservoir age. Though less frequent, these changes may indeed

306   amputate and/or deform a plateau, then as result of variations in local ocean atmosphere

307   exchange and oceanic mixing. Two aspects help to sort out short-term climate-driven

308   intra- and inter-plateau changes in ^{14}C reservoir age: (i) The evaluation of the structure

309   and reservoir age of an individual plateau is strictly including the age estimates deduced

310   for the complete suite of plateaus. (ii) Our experience shows that deglacial climate

311   regimes in control of changes in surface ocean dynamics generally occurred on (multi-)

312   millennial time scales (e.g., YD, B/A, HS-1), whereas atmospheric ^{14}C plateaus hardly

313   lasted longer than a few hundred up to 1100 yr (Fig. 1 and S1). Abrupt changes in gas

314   exchange or ocean mixing usually affect one or only a few plateaus of the suite. --

315   Absolute age estimates within a plateau are derived by linear interpolation between the

316   age of the base and top of an undisturbed plateau assuming constant sedimentation

317   rates. The potential impact of short-term sedimentation pulses on ^{14}C plateau formation

318   has largely been discarded by Balmer and Sarnthein (2016).

319

320   *2.2 Suigetsu atmospheric ^{14}C record: Shift to a chronology based on U/Th model ages*

321   Originally, we based the chronology of ^{14}C plateau boundaries in the Suigetsu record

322   (Sarnthein et al., 2015) on a scheme of varve counts by means of light microscopy of

323   thin sections (Bronk Ramsey et al., 2012; Schlolaut et al., 2018). Over the crucial

324   sediment sections of the Last Glacial Maximum (LGM) and deglacial Heinrich Stadial 1

325   (HS-1), however, varve quality / perceptibility in the Suigetsu profile is highly variable

326   (Fig. 5). In parallel, varve-based age estimates were derived from counting various

327   elemental peaks in µXRF data and interpreted as seasonal signals (Marshall et al.,

328   2012). The results obtained from the two independent counting methods and their

329   interpolations widely support each other but diverge for older ages. The varve counts

330   ultimately formed the backbone of a high-resolution chronology obtained by tying the

331   Suigetsu ^{14}C record to the U/Th based time scale of the Hulu cave ^{14}C record (Bronk

332   Ramsey et al., 2012). Recently, Schlolaut et al. (2018) amended the scheme of varve

333   counts. Accordingly, Suigetsu varve preservation (i.e., the number of siderite layers per

334   20 cm thick sediment section) is fairly high prior to ~32 ky BP and over late glacial

335   Termination I but fairly poor over large parts of the LGM and HS-1, from ~15 – 32 cal ka

336   (17.3-28.5 m c.d. in Fig. 5). Here only less than 20-40 % of the annual layers expected

337   from interpolation between clearly varved sections are distinguished by microscopy.

338   Varve counts that use µXRF data (Marshall et al., 2012) can distinguish subtle changes

339   in seasonal element variations, that are not distinguishable in thin section microscopy,

340   hence result in higher varve numbers especially during early deglacial-to-peak glacial

341   times. Yet, some subtle variations are difficult to distinguish from noise, which adds

342   uncertainty to the µXRF-based counts. Thus, the results from either counting method

343   are subject to uncertainties that rise with increased varve age (Fig. 5).

344

345   Bronk Ramsey et al. (2012) established a third time scale based on ^{14}C wiggle matching

346   to U/Th dated ^{14}C records of the Hulu Cave and Bahama speleothems. In part, this

347   calibrated (cal.) age scale was based on Suigetsu varve counts, in part on the

348   prerequisite of the best-possible fit of a pattern of low-frequency changes in ^{14}C

349   concentration obtained from Suigetsu and Hulu Cave. The two ^{14}C records were fitted

350   within the uncertainty envelope of the Hulu 'Old / Dead Carbon Fraction' (OCF/DCF) of

351   ^{14}C concentration. The uncertainty of this model is still incompletely understood. The

352   U/Th-based age model of Suigetsu may suffer from the wiggle matching of atmospheric

353   ^{14}C ages of Lake Suigetsu with ^{14}C ages of the Hulu Cave (Southon et al., 2012) in case

354   of major short-term changes in atmospheric ^{14}C concentration due to a memory effect of

355   soil organic carbon in carbonate-free regions of the cave overburden. The speleothem-

356   carbonate-based Hulu ages may have been influenced far more strongly by short-term

357   changes in the local DCF than assumed, as suggested by major variations in a paired

358    $\delta^{13}C$ record, that reach up to 5 ‰, mostly subsequent to short-term changes in past

359   monsoon climate (Kong et al., 2005). The uncertainty regarding the assumption of a

360   constant OCF/DCF (Southon et al. 2012; Cheng et al., 2018) may hamper the age

361   model correlation between Hulu and Suigetsu records and the Suigetsu chronology.

362

363   We compared the results of the two timescales, independently deduced from varve

364   counts, with those of the U/Th-based model age scale using as test case the base of

365   ^{14}C Plateau 2b, the oldest tie point constrained by µXRF-based counts. In contrast to

366   16.4 cal. ka, supposed by optical varve counts, µXRF-based counts suggest an age of

367   ~16.9 cal. ka (Marshall et al., 2012; Schlolaut et al., 2018), which matches closely the

368   U/Th-based estimate of 16.93 ka. This is a robust argument for the use of the U/Th-

369   based Suigetsu time scale as 'best possible' age scale to calibrate the age of thirty ^{14}C

370   plateau boundaries (Fig. 1). In its older part, the U/Th model time scale is further

371   corroborated by a decent match of short-term increases in ^{14}C concentration with the

372   low geomagnetic intensity of the Mono Lake and Laschamp events at ~34 and

373   41.1±0.35 ka (Lascu et al., 2016), independently dated by other methods. The new

374   U/Th-based model ages of ^{14}C plateau boundaries are significantly higher than our

375   earlier microscopy-based varve ages over HS-1 and LGM, a difference increasing from

376   ~200 yr near 15.3 cal. ka to ~530 near 17 ka and 2000 yr near ~29 ka (Fig. 3).

377

378   Note, any readjustment of the calendar age of a ^{14}C plateau boundary does not entail

379   any change in ^{14}C reservoir ages afore deduced for surface waters by means of the

380 plateau technique (Sarnthein et al., 2007, 2015), since each reservoir age presents the

381 simple difference in average ^{14}C age for one and the same ^{14}C plateau likewise defined

382 in both the Suigetsu atmospheric and planktic ^{14}C records of marine surface waters,

383 independent of the precise position of this plateau on the calendar age scale.

384

385 In view of the recent revision of time scales (Schlolaut et al., 2018; Bronk Ramsey et al,

386 2019) we now extended our plateau tuning and now also defined the boundaries and

387 age ranges of ^{14}C plateaus and jumps for the interval ~23–29 cal. ka, which results in a

388 total of ~30 atmospheric age tie points for the time span 10.5–29 cal. ka (Fig. 1;

389 summary in Table 1; following the rules of Sarnthein et al., 2007 and 2015). Prior to 25

390 cal. ka, the definition of ^{14}C plateaus somewhat suffered from an enhanced scatter of

391 raw ^{14}C values of Suigetsu. -- In addition to visual inspection, the ^{14}C jumps and

392 plateaus were also defined with higher statistical objectivity by means of the first-

393 derivative of all trends in the ^{14}C age-to-calendar age relationship (or –core depth

394 relationship, respectively) by using a running kernel window (Sarnthein et al., 2015).

395

396 *2.3 Linkages of short-term structures in the atmospheric ^{14}C record to changes in*

397 *cosmogenic ^{14}C production versus changes in ocean dynamics*

398

399 Potential sources of variability in the atmospheric ^{14}C record have first been discussed

400 by Stuiver and coworkers in the context of Holocene fluctuations deduced from tree ring

401 data (e.g., Stuiver and Braziunas 1993), more recently simulated (e.g., Hain et al.,

402 2014). -- Similar to changes in ^{14}C, variations in ^{10}Be deposition in ice cores reflect past

403 changes in ^{10}Be production as a result of changes in solar activity and the strength of

404 the Earth's magnetic field (Adolphi et al., 2018). If we accept to omit assumptions on the

405 modulation of past ^{14}C concentrations by changes in the global carbon cycle we can

406 calculate the atmospheric ^{14}C changes over last glacial-to-deglacial times with ^{10}Be and

407 a carbon cycle model and convert them into ^{14}C ages (Fig. 4). Changes in climate and

408 carbon cycle, however, over this period necessarily modified the ^{10}Be-based ^{14}C record

409 if included correctly into the modeling. Between 10 and 13.5 cal. ka, the ^{10}Be-modeled

410 ^{14}C record displays a number of plateau structures that appear to match the Suigetsu-

411 based atmospheric ^{14}C plateaus. Between 15 and 29 cal. ka, however, ^{10}Be-based ^{14}C

412 plateaus are more rare and/or less pronounced than those in the Suigetsu record. Most

413 modelled plateaus are far shorter than those displayed in the suite of atmospheric ^{14}C

414 plateaus of Lake Suigetsu (e.g., plateaus near to the top 2a, 2b, top 5a, and 9), except

415 for a distinct equivalent of plateau no. 6a. On the whole, the modelled and observed

416 structures show little coherence. This may indicate that any direct relationship between

417 variations in cosmogenic ^{14}C production and the Suigetsu plateau record is largely

418 obscured by the carbon cycle, uncorrected climate effects on the ^{10}Be deposition,

419 and/or noise in the ^{14}C data. Also, a relatively high uncertainty of the measured ^{10}Be

420 concentrations in the ice, (in many cases ~7%; Raisbeck et al., 2017), and a lower

421 sample resolution in the order of 50 to 200 yr may contribute to the smoothed character

422 of the ^{10}Be record in Fig. 4.

423

424 On the other hand, the 'new' U/Th-based cal. ages of plateau boundaries may suggest

425 some reasonable stratigraphic correlations between peak glacial and deglacial change in

426 atmospheric CO_2 and ^{14}C plateaus with millennial-scale events in paleoceanography (Fig.

427 6, Table 2): The suite of deglacial ^{14}C plateaus no. 2a, 1, and Top YD indeed displays a

428 temporal match with three brief but major deglacial jumps in ocean degassing of CO_2

429 documented in the WDC ice core (Marcott et al., 2014). The two records have been

430   independently dated by means of annual-layer counts in ice cores and U/Th ages of

431   stalagmites. The match suggests that these atmospheric ^{14}C plateaus may largely result

432   from changes in air-sea gas exchange, and in turn, from changes in ocean dynamics.

433

434   In particular, these events may have been linked to a variety of fast changes such as in

435   sea ice cover in the Southern Ocean and/or in the salinity and buoyancy of high-latitude

436   surface waters (Skinner et al., 2010; Burke and Robinson, 2012). These factors control

437   upwelling and meridional overturning of deep waters, in particular found in the Southern

438   Ocean (Chen et al., 2015) and/or North Pacific (Rae et al. 2014, Gebhardt et al., 2008).

439   Such events of changes in MOC geometry and intensity may be responsible for ocean

440   degassing and the ^{14}C plateaus. The enhanced mixing of the Southern Ocean and a

441   similar, slightly later mixing event in the North Pacific (MD02-2489; Fig. S2d) may have

442   triggered – with phase lag – two trends in parallel, (1) a rise in atmospheric CO_2, in part

443   abrupt (*sensu* Chen et al., 2015; Menviel et al., 2018), and (2) a gradual enrichment in ^{14}C

444   depleted atmospheric carbon, reflected as ^{14}C plateau.

445

446   Plateau 6a matches a ^{14}C plateau deduced from atmospheric ^{10}Be concentrations, thus

447   suggests changes in ^{14}C production. Other changes in atmospheric ^{14}C (plateaus 4 and

448   8) match short-term North Atlantic warmings during peak glacial and earliest deglacial

449   times, similar to that at the end of HS-1 and during plateau 'YD', hence may reflect

450   minor changes in ocean circulation and ocean-atmosphere exchange without major

451   degassing of old ^{14}C depleted deep waters in the North Atlantic (Table 2, Fig. S2a).

452   There is still little information, however, on the origin of several other peak glacial ^{14}C

453   plateaus 17.5–29 cal. ka. The actual linkages of these plateaus to events in ocean MOC

454   still remain to be uncovered.

455

3. DISCUSSION and IMPLICATIONS

3.1 ^{14}C plateau boundaries – A suite of narrow-spaced age tie points to rate short-term

changes in marine sediment budgets, chemical inventories, and climate 29–10 cal. ka

In continuation of previous efforts (Sarnthein et al., 2007 and 2015) the tuning of high-

resolution planktic ^{14}C records of ocean sediment cores to the new age-calibrated

atmospheric ^{14}C plateau boundaries now makes it possible to establish a 'rung ladder'

of ~30 age tie points covering the time span 29 – 10 cal. ka. These global tie points

have a time resolution of several hundred to thousand years to be used to constrain the

chronology and potential leads and lags of events that occurred during peak glacial and

deglacial times (Fig. 1). The locations of 18 (20; depending on the age range covered)

^{14}C records are shown in Fig. 7. Figs. 8 and S2 give the time histories of the planktic

and benthic reservoir ages, the information they provide is discussed below.

Six prominent examples showing the power and value of additional information obtained

by means of the ^{14}C plateau-tuning method are:

   (i) The timing of ocean signals of the onset of deglaciation (sudden depletion of

planktic δ^{18}O and rise in SST) in the North Atlantic and North Pacific can now be

distinguished in detail from those in the Southern Hemisphere, where warming began at

17.6 cal. ka, when the cooling of Heinrich 1 started in the North Atlantic (Fig. S2)

(Küssner et al., 2020 subm.); in harmony with Schmittner and Lund, 2015), a finding

important to further constrain global 'bipolar see-saw' (Stocker and Johnsen, 2003).

   (ii) Likewise, the end of the cooling equated with the Antarctic Cold Reversal (ACR;

WDC Project Members, 2013) in Pacific surface waters off Central Chile was found

480   precisely coeval with the onset of the Younger Dryas cold spell in the Northern

481   Hemisphere (Küssner et al., 2020 subm.).

482   (iii) Signals of local deep-water formation in the subpolar North Pacific can now be

483   separated from signals originating in the North Atlantic (Rae et al. 2014; Sarnthein et al.,

484   2013). In this way we now can specify and tie major short-lasting reversals in Atlantic

485   and Pacific MOC on a global scale.

486   (iv) Signals of deglacial meltwater advection can now be distinguished from short-

487   term interstadial warmings in the northern subtropical Atlantic, which helps to locate

488   meltwater outbreaks far beyond the well-known Heinrich belt of ice-rafted debris

489   (Balmer and Sarnthein, 2018).

490   (v) As outlined above, the timing of marine ^{14}C plateaus can now be compared in

491   detail with that of deglacial events of climate and the atmospheric CO_2 rise independ-

492   ently dated by means of ice core-based stratigraphy (Table 2; Fig. 6). These linkages

493   offer a tool to explore details of deglacial changes in deep-ocean MOC once the suite of

494   ^{14}C plateaus has been properly tuned at any particular ocean site.

495   (vi) The refined scale of age tie points also reveals unexpected details for changes in

496   the sea ice cover of high latitudes as reflected by anomalously high ^{14}C reservoir ages

497   (e.g. north of Iceland and near to the Azores Islands) and for the evolution of Asian

498   summer monsoon in the northern and southern hemisphere as reflected by periods of

499   reduced sea surface salinity (e.g., Sarnthein et al., 2015; Balmer et al., 2018).

500

501   Finally, the plateau-based high-resolution chronology has led to the detection of

502   numerous millennial-scale hiatuses (e.g., Sarnthein et al., 2015; Balmer et al., 2016;

503   Küssner et al., 2020 subm.) overlooked by conventional, e.g., *AnalySerie*-based

504   methods (Paillard et al. 1996) of stratigraphic correlation (Fig. S2). In turn, the hiatuses

505 give intriguing new insights into past changes of bottom current dynamics linked to

506 different millennial-scale geometries of overturning circulation and climate change such

507 as in the South China Sea (Sarnthein et al., 2013 and 2015), in the South Atlantic

508 (Balmer et al. 2016) and southern South Pacific (Ronge et al., 2019).

509

510 Clearly, the new atmospheric ^{14}C 'rung ladder' of closely-spaced chronostratigraphic tie

511 points has evolved to a valuable tool to uncover functional chains in paleoceanography,

512 that actually have controlled events of climate change over glacial-to-deglacial times.

513 The extension of the age range back to 29 ka allows constraining potential changes in

514 the ocean dynamics expected for Dansgaard Oeschger (DO) events 2, 3, and 4 as

515 compared to those found for DO-1, though pertinent core records are still missing.

516

517 *3.2 Observed vs. model-based ^{14}C reservoir ages that act as tracer of past changes in*

518 *surface ocean dynamics provide incentive for model refinements*

519

520 Radiocarbon plateau tuning of marine sediment sections to the Suigetsu ^{14}C

521 atmospheric master record allows us to establish at semi-millennial-scale resolution the

522 difference between the average ^{14}C age of coeval atmospheric and planktic ^{14}C

523 plateaus. The suite of changing ^{14}C reservoir ages over time forms a prime tracer of

524 past ocean dynamics influencing local surface waters and a data set crucial to deduce

525 past apparent deep-water ventilation ages (e.g., Muglia et al., 2018; Cook and Keigwin,

526 2015; Balmer and Sarnthein, 2018).

527

528 To better constrain the water depth of past reservoir ages we dated monospecific

529 planktic foraminifera (Sarnthein et al., 2007); in low-to-mid latitudes on *G. bulloides*, *G.*

ruber, or *G. sacculifer* with habitat depths of 0–80/120 m (Jonkers and Kucera, 2017) and in high latitudes, mostly on *N. pachyderma* (s) living at 0–200 m depth (Simstich et al., 2003). Averaging of ^{14}C ages within a ^{14}C plateau helps to remove analytical noise and minor real ^{14}C fluctuations. Nine plateaus are located in the LGM, 18–27 cal. ka (Fig. 1). Here, planktic foraminifera-based reservoir ages show analytical uncertainties of >200 to >300 yr each for standard AMS dating. By comparison, short-term temporal variations in reservoir age reach 200–400 yr, occasionally up to 600 yr, in particular, close to the end of the LGM (Table 3).

To better decode the informative value of our ^{14}C reservoir ages for late LGM we compared average ages of [14]C Plateaus 4-5 (18.6–20.9 cal. ka) with estimates generated by various global ocean models, an approach similar to that of Toggweiler et al. (2019) applied to modern reservoir ages of the global ocean. In an earlier paper (Balmer et al., 2016) we compared our empiric reservoir ages for the LGM with GCM-based estimates of Franke et al. (2008) and Butzin et al. (2012). Franke et al. (2008) underestimated our mid-latitude values by up to ~2000 ^{14}C yr, while LGM reservoir age estimates of Butzin et al. (2012) were more consistent with ours. Their GCM considered more realistic boundary conditions such as the LGM freshwater balance in the Southern Ocean and, in particular, LGM SST and wind fields plus the gas transfer velocity for the exchange of ^{14}C of CO_2 (Sweeney et al., 2007). Further improvements are expected from a model configuration that properly resolves the topographic details of the continental margins and adjacent seas, which frequently form the origin of our sediment-based data sets (Butzin et al., 2020). For the time being, we compared our empirical estimates with estimates from a coarse-resolution GCM, using the results by Muglia et al. (2018; 0–50 m w.d.; Fig. 8c-d; Table 3) as an example. Their model

555   includes ocean surface reservoir age and ocean radiocarbon fields that have been

556   validated through a comparison to LGM ^{14}C data compilation made by Skinner et al.

557   2017. It conforms two plausible, recent model estimates of surface reservoir ages that

558   can be compared to our results (Table 3).

559

560   Low LGM values (300–750 yr) supposedly document an intensive exchange of surface

561   waters with atmospheric CO_2, most common in model- and foraminifera-based

562   estimates of the low- and mid-latitude Atlantic. Low empiric values also mark LGM

563   waters in mid to high latitudes off Norway and off middle Chile, that is, close to sites of

564   potential deep and/or intermediate water formation. Off Norway and in the northeastern

565   Atlantic, model-based reservoir ages of Muglia et al. (2018) largely match the empiric

566   range. However, the uncertainty envelopes for data shown in Fig. 8c (±560 yr; r = 0.59)

567   generally exceed by far the spatial differences calculated for the empiric data.

568   Conversely, model-based reservoir ages reproduce only poorly the low planktic

569   foraminifera-based estimates off Central Chile and values in the Western Pacific and

570   Southern Ocean.

571   In part, the differences may be linked to problems like insufficient spatial resolution

572   along continental margins, ignoring east-west differences within ocean basins, and/or

573   the estimates of a correct location and extent of seasonal sea ice cover used as LGM

574   boundary condition such as east off Greenland, in the subpolar northwest Pacific, and

575   off Southern Chile, where sea ice hindered the exchange of atmospheric carbon (per

576   analogy to that of temperature exchange, e.g., Sessford et al, 2019). Also, model

577   estimates of the annual average are compared to ^{14}C signals of planktic foraminifera

578   that mostly formed during summer only, e.g., when large parts of the Nordic Seas were

579   found ice-free (Sarnthein et al., 2003). Hence, models may need to better constrain

580   local and seasonal sealing effects of LGM sea ice cover.

581

582   In general, the foraminifera-based reservoir age estimates for our sites that represent

583   various hydrographic key regions in the high-latitude ocean appear much higher than

584   model-derived values. These deviations reach up to 1400 yr, in particular in the

585   Southern Ocean. In part, they may result from the fact that present models may not yet

586   be suited to capture small-scale ocean structures such as the interference of ocean

587   currents with local bathymetry and local upwelling cells. Here, model-based reservoir

588   ages appear far too low in LGM regions influenced by regional upwelling such as the

589   South China Sea then governed by an estuarine overturning system (Wang et al., 2005;

590   Fig. 9), by coastal upwelling off N.W. Australia (Xu et al., 2010; Sarnthein et al., 2011),

591   or by a melt water lid such as off eastern New Zealand (Bostock et al., 2013; Küssner et

592   al., 2020 subm.). Local oceanic features are likely to be missed in current resolution

593   models. Our more narrow-spaced empiric data could help to refine the skill of models to

594   capture past ^{14}C reservoir ages.

595

596   Various differences amongst plankton- and model-based reservoir ages may also result

597   from differential seasonal habitats of the different planktic species analyzed that, in turn,

598   may trace different surface and subsurface water currents. Distinct interspecies

599   differences were found in Baja California that record differential, upwelling-controlled

600   habitat conditions (Lindsay et al, 2015). In the northern Norwegian Sea interspecies

601   differences amount up to 600 yr for the Preboreal ^{14}C plateau, 9.6–10.2 cal. ka

602   (Sarnthein and Werner, 2018). Here ^{14}C records of Arctic *Turborotalita quinqueloba*,

603   dominantly grown close to the sea surface during peak summer, differ from the paired

604 record of *Neogloboquadrina pachyderma*, formed in subsurface waters, and that of

605 subpolar species *N. incompta*, mainly advected from the south by Norwegian Current

606 waters well mixed with the atmosphere during peak winter. This makes closer

607 specification of model results as product of different seasonal extremes a further target.

608

609 *3.3 Planktic foraminifera-based ^{14}C reservoir ages – A prime database to estimate past*

610 *changes in the ^{14}C ventilation age of deep waters and past oceanic MOC and DIC*

611

612 'Raw' apparent benthic ventilation ages (in ^{14}C yr; 'raw' *sensu* Balmer et al., 2018)

613 express the difference between the (coeval) atmospheric and benthic ^{14}C levels

614 measured at any site and time of foraminifer deposition. These ages are the sum of (1)

615 the planktic reservoir age of the ^{14}C plateau that covers a group of paired benthic and

616 planktic ^{14}C ages and (2) the (positive or negative) ^{14}C age difference between any

617 benthic ^{14}C age and the average ^{14}C age of the paired planktic ^{14}C plateau. The benthic

618 ventilation ages necessarily rely on the high quality of ^{14}C plateau-based chronology,

619 since the atmospheric ^{14}C level has been subject to substantial short-term changes over

620 glacial-to-deglacial times. Necessarily, the ventilation ages include a mixing of different

621 water masses that might originate from different ocean regions and may contribute

622 differential ^{14}C ventilation ages, an unknown justifying the modifier 'apparent'.

623

624 In a further step, the $\Delta\Delta^{14}$C equivalent of our 'raw' benthic ventilation age may be

625 adjusted to changes in atmospheric ^{14}C that occurred over the (short) time span

626 between deep-water formation and benthic sediment deposition (e.g., Balmer and

627 Sarnthein, 2018; Cook and Keigwin, 2015). In most cases, however, this second step is

628 omitted since its application usually does not imply any major modification of the

629 ventilation age estimates (Fig. S2a; Skinner et al., 2017; Sarnthein et al., 2013).

630

631 On the basis of ^{14}C plateau tuning we now can rely on 18 accurately dated records of

632 apparent benthic ^{14}C ventilation ages (Fig. S2a-d) to reconstruct the global geometry of

633 LGM and HS-1 deep and intermediate water circulation as summarized in ocean

634 transects and maps (Figs. 9–11) and discussed below. The individual matching of our

635 20 planktic ^{14}C plateau sequences with that of the Suigetsu atmospheric ^{14}C record is

636 displayed in Sarnthein et al. (2015), Balmer et al., (2016), Küssner et al. (2020 subm.),

637 and Ausin et al. (2020 subm.). In addition, robust estimates of past reservoir ages are

638 obtained for 4 planktic and benthic ^{14}C records from paired atmospheric ^{14}C ages of

639 wood chunks (Rafter et al., 2018; Zhao and Keigwin, 2018; Broecker et al., 2004).

640

641 *3.3.1 — Major features of ocean meridional overturning circulation during LGM (Fig. 10)*

642

643 Off Norway and near the Azores Islands very low benthic ^{14}C ventilation ages of <100–

644 750 yr suggest ongoing deep-water formation in the LGM northern North Atlantic

645 reaching down to more than 3000–3500 m water depth, with a flow strength possibly

646 similar to today (and a coeval deep countercurrent of old waters from the Southern

647 Ocean flowing along the East Atlantic continental margin off Portugal). This pattern

648 clearly corroborates the assembled benthic δ^{13}C record showing plenty of elevated δ^{13}C

649 values for the northwestern, eastern and central North Atlantic (Sarnthein et al., 1994;

650 Millo et al., 2006; Keigwin and Swift, 2017). Irrespective of unspecified potential zonal

651 variations in deep-water ventilation age at mid latitudes and different from a number of

652 published models (e.g., Ferrari et al., 2014; Butzin et al., 2017) this 'anti-estuarine'

653   pattern has been confirmed by a global tracer transport model of Gebbie (2014),

654   MIROC model simulations (Sherriff-Tadano et al., 2017, Yamamoto et al., 2019), and

655   independently, by ε_{Nd} records (Howe et al., 2016; Lippold et al., 2016). The latter

656   suggest an overturning of AMOC possibly even stronger than today, in particular due to

657   a 'thermal threshold' (Abé-Ouchi, 2018) overlooked in other model simulations.

658

659   In contrast to the northern North Atlantic, deep waters in the southern North Atlantic and

660   Circumpolar (CP) deep waters in the subpolar South Atlantic show an LGM [14]C

661   ventilation age of ~3640 yr, finally rising up to 3800 yr (Figs. 10, 11, S2b). These waters

662   were upwelled and admixed from below to surface waters near to the sub-Antarctic

663   Front during terminal LGM (Fig. S2b; Skinner et al., 2010; Balmer and Sarnthein, 2016;

664   model of Butzin et al., 2012).

665

666   In the southwestern South Pacific abyssal, in part possibly Antarctic-sourced waters

667   (Rae and Broecker, 2018) likewise show high apparent ^{14}C ventilation ages of 3500 yr

668   that drop to 2750 yr near the end of the LGM (Figs. 10 top and S2c) (^{14}C dates of

669   Ronge et al., 2016, modified by planktic ^{14}C reservoir ages of Küssner et al., 2020

670   subm.). A vertical transect of benthic $\delta^{13}C$ (McCave et al., 2008) suggests that the

671   abyssal waters were overlain by CP waters, separated by pronounced stratification near

672   ~3500–4000 m water depth. In part, the CP waters stemmed from North Atlantic Deep

673   Water. Probably, their apparent ventilation age 3500 yr came close to the values found

674   in the southern South Atlantic. East of New Zealand the CP waters entered the deep

675   western Pacific and spread up to the subpolar North Pacific, where LGM ^{14}C ventilation

676   ages reached ~3700 yr, possibly occasionally 5000 yr (Fig. S2d).

677

678 Similar to today, the MOC of the LGM Pacific was shaped by estuarine geometry,

679 probably more weakened than today (Du et al., 2018) and more distinct in the far

680 northwest than in the far northeast. This geometry resulted in an upwelling of old deep

681 waters in the subarctic Northwest Pacific, here leading to a ^{14}C reservoir age of ~1700

682 yr for surface waters at terminal LGM. On top of the Lower Pacific Deep Waters we may

683 surmise Upper Pacific Deep Waters that moved toward south (Figs. 10 top and 11).

684

685 The Pacific deep waters were overlain by Antarctic / Pacific Intermediate Waters (IW)

686 with LGM ^{14}C ventilation ages as low as 1400–1800 yr, except for a shelf ice-covered

687 site at the southern tip of Chile with IW ages of 2400–2900 yr, possibly a result of local

688 upwelling of CP waters. In general, however, the low values of Pacific IW are similar to

689 those estimated for South Atlantic IW and likewise reflect a vivid exchange with

690 atmospheric CO_2 in their source regions in the Southern Ocean (Skinner et al., 2015).

691

692 When entering and crossing the entrance sill to the marginal South China Sea the

693 'young' IW were mixed with 'old' CP waters entrained from below, here leading to ^{14}C

694 ventilation ages of 2600–3450 yr (Figs. 9 and S2d). The LGM South China Sea was

695 shaped by an estuarine-style overturning system marked by major upwelling near to its

696 distal end in the far southwest (Wang L. et al., 1999). This upwelling led to planktic ^{14}C

697 reservoir ages as high as 1200–1800 yr, values rarely found elsewhere in surface

698 waters of low latitudes.

699

700 Our wide-spaced distribution pattern of 18 open-ocean ^{14}C ventilation ages (plus 4

701 values based on paired wood chunks) in Figs. 10 and 11 agrees only in part with the

702 circulation patterns suggested by the much larger datasets of ^{14}C ventilation ages

703   compiled by Skinner et al. (2017) and Zhao et al. (2018). Several features in Figs. 10

704   and 11 directly deviate, e.g., the ages we derive for the North Atlantic and mid-depth

705   Pacific. These deviations may be linked to both the different derivation of our ^{14}C

706   ventilation age estimates and the details of our calendar-year chronology now based on

707   the narrow-standing suite of ^{14}C plateau-boundary ages. The quality of our ^{14}C reservoir

708   ages of surface waters also controls the 'apparent' ventilation age of deep-waters, as it

709   results from direct addition of the short-term average ^{14}C age of a planktic ^{14}C plateau to

710   a paired, that is coeval benthic ^{14}C age (formed during the time of benthic foraminiferal

711   growth, somewhat after the actual time of deep-water formation).

712

713   *3.3.2 — Major features of meridional overturning circulation during early HS-1 (Fig. 10)*

714

715   Near the onset of deglacial Heinrich Stadial 1 (HS-1; ~18–14.7 cal. ka) major shifts in

716   ^{14}C ventilation age suggest some short-lasting but fundamental changes in the

717   circulation geometry of the deep ocean, a central theme of marine paleoclimate

718   research (lower panel of Figs. 10, 11 and S2a and b). Deep waters in the eastern

719   Nordic Seas, west of the Azores Islands, and off northern Brazil show a rapid rise to

720   high ^{14}C ventilation ages of ~2000–2500 yr and up to 4000 yr off Brazil, values that give

721   first proof for a brief switch from 'anti-estuarine' to 'estuarine' circulation that governed

722   the central North Atlantic and Norwegian Sea during early HS-1. This geometry

723   continued – except for a brief but marked and widespread event of recurring NADW

724   formation near 15.2 ka – until the very end of HS-1 near 14.5 ka (Fig. S2a; Muschitiello

725   et al., 2019). The MOC switch from LGM to HS-1 is in line with changes depicted in

726   paired benthic δ^{13}C data (Sarnthein et al., 1994), but not confirmed by the coeval ε_{Nd}

727   record that suggests a constant source of 'mid-depth waters', with the δ^{13}C drop being

728   simply linked to a higher age (Howe et al., 2018).

729

730   Conversely, benthic ^{14}C ventilation ages in the northeastern North Pacific (Site MD02-

731   2489) show a coeval and distinct but brief minimum of 1050-1450 yr near 3640 m w.d.

732   during early HS-1 (~18.1–16.8 ka; Figs. 10, 11, and S2d). This minimum was produced

733   by extremely small benthic-planktic age differences of 350–650 yr and provides robust

734   evidence for a millennial-scale event of deep-water formation, that has flushed the

735   northeastern North Pacific down to more than 3640 m w.d. (Gebhardt et al., 2008;

736   Sarnthein et al., 2013; Rae et al., 2014). Similar circulation geometries were reported for

737   the Pliocene (Burls et al., 2017). 'Young' Upper North Pacific Deep Waters (North

738   Pacific Intermediate Waters *sensu* Gong et al., 2019) then penetrated as 'western

739   boundary current' far south, up to the northern continental margin of the South China

740   Sea (Figs. 9b, 11, and S2d). The short-lasting North Pacific regime of anti-estuarine

741   overturning was similar to that we find in the modern and LGM Atlantic and, most

742   interesting, simultaneous with the Atlantic's estuarine episode.

743

744   Recent data on benthic-planktic ^{14}C age differences (Du et al., 2018) precisely recover

745   our results in a core at ~680 m w.d. off southern Alaska. However, they do not depict

746   the 'young' deep waters at their Site U1418 at ~3680 m w.d., as corroborated by a

747   paired autigenic ε_{Nd} maximum suggesting a high local bottom water age nearby. We

748   assume that the amazing difference in local deep-water ventilation ages is due to small-

749   scale differences in the effect of Coriolis forcing at high latitudes between a site located

750   directly at the base of the Alaskan continental margin (U1418; Fig. 10b) and that on the

751   distal Murray Sea Mount in the 'open' Pacific (MD02-2489; Figs. 7 and 11), which

752   probably has been been washed by a plume of newly formed North Pacific deep waters

753   probably stemming from the Bering and/or Ochotsk Seas. In contrast, the incursion of

754   almost 3000 yr old deep waters from the Southern Ocean has continued along the

755   continental margin all over HS-1. In summary we may conclude that the geometry of

756   ocean MOC was briefly reversed in the 'open' North Pacific over almost 1500 years

757   during HS-1, far deeper than suggested by previous authors (e.g., Okazaki et al., 2012;

758   Gong, S., et al. 2019), but similar to changes in geometry first proposed by Broecker et

759   al. (1985) then, however, for an LGM ocean.

760

761   *3.3.3 — Deep-Ocean DIC inventory*

762

763   Apart from the changing geometries in ocean MOC during LGM and HS-1, the global

764   set of ^{14}C plateau-based, hence refined estimates of apparent ^{14}C ventilation ages (Fig.

765   10) has ultimately also revealed new insights into glacial-to-deglacial changes in deep-

766   ocean DIC inventories (Sarnthein et al., 2013; Skinner et al., 2019). On the basis of

767   GLODAP data (Key et al., 2004) any drop in ^{14}C concentration (i.e., any rise in average

768   ^{14}C ventilation age) of modern deep waters is tied linearly to a rise of carbon (DIC)

769   dissolved in deep ocean waters below ~2000 m, making for 1.22 micromole C / -1 ‰

770   ^{14}C. By and large, GCM and box model simulations of Chikamoto and Abé-Ouchi (2012)

771   and Wallmann et al. (2016) suggest that this ratio may also apply to LGM deep-water

772   circulation, when apparent ^{14}C ventilation ages in the Southern Ocean increased

773   significantly (from 2400 up to ~3800 yr) and accordingly, thermohaline circulation was

774   more sluggish and transit times of deep waters extended. Accordingly, a 'back-of-the-

775   envelope' calculation of LGM ventilation age averages in the global deep ocean

776   suggests an additional carbon absorption of 730–980 Gt (Sarnthein et al., 2013). This

777 estimate can easily accommodate the glacial transfer of ~200 Gt C from the atmosphere

778 and biosphere, moreover, may also explain 200–450 Gt C then most probably removed

779 from glacial Atlantic and Pacific intermediate waters. These estimates offer an

780 independent evaluation of ice core-based data, other proxies, and model-based data on

781 past changes in the global carbon cycle (e.g., Menviel et al., 2018).

782

783 4. SOME CONCLUSIONS AND PERSPECTIVES

784 – Despite some analytical scatter, ^{14}C ages for the top and base of Lake Suigetsu-

785 based atmospheric ^{14}C plateaus and coeval planktic ^{14}C plateaus do not present

786 statistical 'outliers' but real age estimates that are reproduced by tree ring-based [14]C

787 ages over the interval 10–13 cal. ka and further back.

788 – Hulu U/Th model-based ages of ^{14}C plateau boundaries of the Suigetsu atmospheric

789 ^{14}C record appear superior to those derived from microscopy-based varve counts only,

790 since U/Th model-based ages match far more closely the age when now deduced from

791 XRF-based varve counts for the tie point of lower plateau boundary 2b, a test case in

792 the early deglacial, and for the age assigned to the Laschamp event prior to the LGM.

793 – During deglacial times, we show that several atmospheric ^{14}C plateaus paralleled a

794 rise in air-sea gas exchange, and, in turn, distinct changes in ocean MOC. Changes in

795 cosmogenic ^{14}C production rarely provide a complete explanation for the plateaus

796 identified in the Suigetsu ^{14}C data under discussion.

797 – In total, ^{14}C plateau boundaries in the range now provide a suite of ~30 age tie points

798 to establish – like chronological ladder rungs – a robust global age control for deep-sea

799 sediment sections and global stratigraphic correlations of last glacial to deglacial climate

800 events, 29–10 cal. ka. U/Th model ages confine the cal. age uncertainty of Suigetsu

801 plateau boundaries assigned halfway between two ^{14}C ages nearby inside and outside

802   a plateau's scatter band to less than ±50 to ±70 yr. Nevertheless, stratigraphic gaps

803   may hamper the accurate tuning of planktic ^{14}C plateaus to their atmospheric

804   equivalents hence result in major discrepancies.

805   – The difference in ^{14}C age between coeval atmospheric and planktic ^{14}C plateaus

806   presents a robust tracer of planktic ^{14}C reservoir ages and shows their high temporal

807   and spatial variability for the LGM and HS-1, now established for 18/20 sediment sites.

808   – Paired reservoir ages obtained from different planktic species document the local

809   distribution patterns of different surface water masses and prevailing foraminiferal

810   habitats at different seasons yet insufficiently considered in model simulations.

811   – New, more robust deep-water ^{14}C ventilation ages, derived on the basis of our robust

812   planktic ^{14}C reservoir ages, reveal geometries of LGM overturning circulation similar to

813   those of today. In contrast, ^{14}C ventilation ages of early HS-1 suggest an almost 1500 yr

814   long event of widely reversed circulation patterns marked by deep-water formation and

815   brief flushing of the northern North Pacific and estuarine circulation geometry in the

816   northern North Atlantic.

817   – Increased glacial ^{14}C ventilation ages and carbon (DIC) inventories of ocean deep

818   waters suggest an LGM drawdown of about 850 Gt C into the deep ocean. Starting with

819   HS-1 a drop of ventilation age suggests carbon released to the atmosphere (Sarnthein

820   et al., 2013).

821   – Site-specific comparison of planktic and model-based reservoir ages estimates

822   highlights the need for further model refinements to make them better reflect the real

823   complex patterns of ocean circulation, including seasonality.

824

825   ACKNOWLEDGMENTS

826 We owe sincere thanks for plenty of stimulations to the 23rd International Radiocarbon

827 Conference in Trondheim, in particular to M-J. Nadeau, and to the IPODS–OC3

828 workshop in Cambridge U.K, 2018, convened by A. Schmittner and L. Skinner.

829 Moreover, we thank for most valuable basic discussions with R. Staff, Glasgow, J.

830 Southon, Irvine CA, and M. Butzin, AWI Bremerhaven, who kindly helped us to discuss

831 the comparison of his model results, and S. Beil, Kiel, for computer assistance. Over the

832 last three years, G. Mollenhauer measured with care hundreds of supplementary ^{14}C

833 ages in her MICADAS laboratory at AWI Bremerhaven. This study obtained long lasting

834 special support from R. Tiedemann and his colleagues at the AWI Bremerhaven.

835

Author contribution

837 All authors contributed data and valuable suggestions to write up this synthesis. MS and

838 PG designed the outline of this manuscript. KK, BA, TE and MS provided new marine

839 ^{14}C records in addition to records previously published. GS displayed the details of

840 Suigetsu varve counts. RM provided a ^{10}Be-based ^{14}C record and plots of raw ^{14}C data

841 sets of Suigetsu und Hulu Cave. Discussions amongst PG, RM, GS and MS served to

842 select U/Th-based model ages as best-possible time scale. JM streamlined the sections

843 on data-model intercomparison.

844

Data availability

846 Published primary radiocarbon data of all sites are available at PANGAEA de. ^{14}C data

847 of 5 marine cores still under publication by Küssner et al. (2020 subm.) and Ausin et al.

848 (subm.; also see caption of Fig. S2) are deposited at PANGAEA.

849

850 REFERENCES (101)

851   Abé-Ouchi, A.: Deglaciation and DO-like experiments with MIROC AOGCM.

852 Abstract, IPODS/OC3 -Workshop on 'Ocean circulation and carbon cycling during the

853 last deglaciation: Global synthesis'. Cambridge 2018.

854   Adkins, J. F. and Boyle, E. A.: Changing atmospheric $\Delta^{14}C$ and the record of

855   paleoventilation ages. Paleoceanography, 12(3), 337–344, 1997.

856   Adolphi, F., Bronk Ramsey, C., Erhard, T., Lawrence Edwards, R., Cheng, H.,

857   Turney, C.S.M., Cooper, A., Svensson, A., Rasmussen, S.O., Fischer, H., and

858   Muscheler, R.: Connecting the Greenland ice-core and U/Th timescales via cosmogenic

859   radionuclides: testing the synchroneity of Dansgaard–Oeschger events. Clim. Past, 14,

860   1755–1781. https://doi.org/10.5194/cp-14-1755-2018, 2018.

861   Alves, E.Q., Macario, K., Ascough, P., and Bronk Ramsey, C.: The worldwide

862   marine radiocarbon reservoir effect: definitions, mechanisms, and prospects. Review of

863   Geophysics, 56, https://doi.org/10.1002/2017RG000588, 2018.

864   Alveson, E.Q.: Radiocarbon in the Ocean, EOS, 99,

865   https://doi.org/10.1029/2018EO095429, 2018.

866   Ausin, B., Haghipour, N., Wacker, L., Voelker, A. H. L., Hodell, D., Magill, C., et al.:

867   Radiocarbon age offsets between two surface dwelling planktonic foraminifera species

868   during abrupt climate events in the SW Iberian margin. Paleoceanography and

869   Paleoclimatology, 34. https://doi.org/10.1029/2018PA003490, 2019.

870   Ausin, B., Sarnthein, M., Haghipour, N., Lougheed, B., Wacker, L., and Eglinton,

871   T.J.: Glacial-to-deglacial radiocarbon history at the southwest Iberian margin.

872   Paleoceanography and Paleoclimate, 2020 subm.

873   Balmer, S., Sarnthein, M., Mudelsee, M., and Grootes, P. M.: Refined modeling and

874   ^{14}C plateau tuning reveal consistent patterns of glacial and deglacial ^{14}C reservoir ages

875   of surface waters in low-latitude Atlantic. Paleoceanography, 31.

876   https://doi.org/10.1002/2016PA002953, 2016.

877   Balmer, S. and Sarnthein, M.: Planktic ^{14}C plateaus, a result of short-term

878   sedimentation pulses? – Radiocarbon, 58, DOI:10.1017/RDC.2016.100, 11 pp., 2016.

879   Balmer, S. and Sarnthein, M.: Glacial-to deglacial changes in North Atlantic melt-

880   water advection and deep-water formation – Centennial-to-millennial-scale ^{14}C records

881   from the Azores Plateau. Geochim. Cosmochim. Acta, 236, 399-415,

882   https://doi.org/10.1016/j.gca.2018.03.001, 2018.

883   Berger W.H. and Keir, R.S.: Glacial-Holocene changes in atmospheric CO_2 and the

884   deep-sea record. J.E. Hansen, T. Takahashi (Eds.), Geophysical Monograph, 29,

885   American Geophysical Union, Washington, DC, pp. 337–351, 1984.

886   Bostock, H.C., Barrows, T.T., Carter, L., Chase, Z., Cortese, G., et al.: A review of

887   the Australian – New Zealand sector of the Southern Ocean over the last 30 ka (Aus-

INTIMATE project). Quaternary Science Reviews 74, 35-57, 2013.

Broecker W.S, Peteet, D.M., and Rind, D.: Does the ocean-atmosphere system have more than one stable mode of operation? Nature, **315**, 21-26, doi:10.1038/315021a0, 1985

Broecker W.S., Barker, S., Clark, E., Hajdas, I., Bonani, G., and Stott, L.: Ventilation of the Glacial deep Pacific Ocean, Science, 306, 1169–1172, 2004.

Bronk Ramsey, C., Staff, R. A., Bryant, C. L., Brock, F., Kitagawa, H., van der Plicht, J., Schlolaut, G., Marshall, M. H., Brauer, A., Lamb, H. F., Payne, R. L., Tarasov, P. E., Haraguchi, T., Gotanda, K., Yonenobu, H., Yokoyama, Y., Tada, R., and Nakagawa, T.: A complete terrestrial radiocarbon record for 11.2 to 52.8 kyr B.P., Science, 338, 370–374, 2012.

Bronk Ramsey, C., Heaton, T.J., Schlolaut, G., Staff, R.A., Bryant, C.L., Lamb, H.F., Marshall, M.H., Nakagawa, T.: Reanalysis of the atmospheric radiocarbon calibration record from Lake Suigetsu, Japan. Radiocarbon, https://doi.org/10.1017/RDC.2020.18, 2020

Burke, A. and Robinson, L.F.: The Southern Ocean's role in carbon exchange during the last deglaciation. Science, 335, 557-561, 2012.

Burls, N.J., Fedorov, A.V., Sigman, D.M., Jaccard, S.L., Tiedemann, R., and Haug, G.H.: Active Pacific meridional overturning circulation (PMOC) during the warm Pliocene. Sci. Adv. 2017;3: e1700156, 2017.

Butzin, M., Prange, M., Lohmann, G.: Radiocarbon simulations for the glacial ocean: The effects of wind stress, Southern Ocean sea ice and Heinrich events. Earth Planet. Sci. Lett., 235, 45-61, 2005.

Butzin, M., Prange, M., and Lohmann, G.: Readjustment of glacial radiocarbon chronologies by self-consistent three-dimensional ocean circulation modeling. Earth Planet Sci. Lett., 317, 177-184, 2012.

Butzin, M., Köhler, P., and Lohmann, G.: Marine radiocarbon reservoir age simulations for the past 50,000 years. Geophys. Res. Lett., 44, 8473–8480, doi:10.1002/2017GL074688, 2017.

Butzin, M., Heaton, T.J., Köhler, P., and Lohmann, G.: A short note on marine reservoir age simulations used in INTCAL20. Radiocarbon, oo, 1-7, DOI:10.1017/RDC.2020.9, 2020.

Chen, T., Robinson, L.F., Burke, A., Southon, J., Spooner, P., Morris, P.J., and Ng, H.C.: Synchronous centennial abrupt events in the ocean and atmosphere during the

last deglaciation, Science, 349, 1537-1541, 2015.

Cheng, H., Edwards, R.L., Southon, J., Matsumoto, K., Feinberg, J.M., Sinha, A., Zhou, W., Li, H., Li, X., Xu, Y., Chen, S., Tan, M., Wang, Q., Wang, Y., and Ning, Y.: Atmospheric 14C/12C changes during the last glacial period from Hulu Cave, Science, 362, 1293-1297, 2018.

Chikamoto, M.O., Abé-Ouchi, A., Oka, A., Ohgaito, R., and Timmermann, A.: Quantifying the ocean's role in glacial CO_2 reductions, Climate of the Past, 8, 545–563, doi:10.5194/cp-8-545-2012, 2012.

Cook M.S. and Keigwin L.D.: Radiocarbon profiles of the NW Pacific from the LGM and deglaciation: Evaluating ventilation metrics and the effect of uncertain surface reservoir ages, Paleoceanography, 30, 174–195, 2015.

Davies, S.M., Davies, P.M., Abbott, Meara, R.H., et al.: A North Atlantic tephro-stratigraphical framework for 130-60 ka b2k: New tephra discoveries, marine based correlations, and future challenges, Quaternary Science Rev., 106, 101-121, 2014.

Du, J., Haley, B.A., Mix, A.C., Walczak, M.H., and Praetorius, S.K.: Flushing of the deep Pacific Ocean and the deglacial rise of atmospheric CO_2 concentrations, Nature geoscience, 11, 749-755, 2018.

Ferrari, R., Jansen, M.F., Adkins, J.F., Burke, A., Stewart, A.L., and Thompson, A.F.: Antarctic sea ice control on ocean circulation in present and glacial climates, Proc. National Academy Science, 111 (24), 8753–8758, 2014.

Gebbie, G.: How much did Glacial North Atlantic Water shoal? Paleoceanography, 29, 190-209, doi:10.1002/2013PA002557, 2014.

Gebhardt, H., Sarnthein, M., Kiefer, T., Erlenkeuser, H., Schmieder, F., and Röhl, U.: Paleonutrient and productivity records from the subarctic North Pacific for Pleistocene glacial terminations I to V. Paleoceanography 23, PA4212, 1-21, doi:10.1029/2007PA001513, 2008.

Gong, S., Lembke-Jene, L., Lohmann, G., Knorr, G., Tiedemann, R., Zou, J.J and Shi, X.F.: Enhanced North Pacific deep-ocean stratification by stronger intermediate water formation during Heinrich Stadial 1. Nature Communications, 10: 656. https://doi.org/10.1038/s41467-019-08606-2, 2019.

Grootes P.M. and Stuiver, M.: Oxygen 18/16 variability in Greenland snow and ice with 1000 to 100000 year time resolution, J. Geophys. Res.: Oceans (1978–2012) 102(C12), 26455–26470, 1997.

955   Grootes, P.M. and Sarnthein, M.: Marine ^{14}C reservoir ages oscillate, PAGES News,

956   14/3, 18-19, 2006.

957   Hain, M.P., Sigman, D.M., and Haug, G.H.: Distinct roles of the Southern Ocean and

958   North Atlantic in the deglacial atmospheric radiocarbon decline, Earth Planetary Science

959   Letters 394, 198-208, 2014.

960   Howe, J.N.W., Piotrowski, A.M., Noble, T.L., Mulitza, S., Chiessi, C.M., and Bayon,

961   G.: North Atlantic deep-water production during the last glacial maximum, Nat.

962   Commun., 7, 11765, 2016. s

963   Howe, J.N.W., Huang, K-F., Oppo, D.W., Chiessi, C.M., Mulitza, S., Blusztajn, J.,

964   and Piotrowski, A.M.: Similar mid-depth Atlantic water mass provenance during the Last

965   Glacial Maximum and Heinrich Stadial 1, Earth Planetary Science Letters, 490, 51-61,

966   2018.

967   Jonkers, L. and Kucera, M.: Quantifying the effect of seasonal and vertical habitat

968   tracking on planktonic foraminifera proxies, Climate of the Past, 13, 573-586, 2017.

969   Keigwin, L.D. and Swift, S.A.: Carbon isotope evidence for a northern source of

970   deep water in the glacial western North Atlantic, PNAS, 114 (11), 2831-2835, 2017.

971   Key R. M., Kozyr, A., Sabine, C.L., Lee, K., Wanninkhof, R., Bullister, J.L., Feely,

972   R.A., Millero, F.J., Mordy, C., and Peng, T.-H. (2004) A global ocean carbon climat-

973   ology: Results from Global Data Analysis Project (GLODAP), Global Biogeochem. Cy.,

974   18, GB4031, doi:10.1029/2004GB002247, 2004.

975   Kong, X., Wang, Y., Wu, J., Cheng, H., Edwards, R.L., and Wang, X.: Complicated

976   responses of stalagmite δ^{13}C to climate change during the last glaciation from Hulu

977   Cave, Nanjing, China, Science in China Ser. D Earth Sciences, 48, (12), 2174-2181,

978   2005.

979   Küssner, K., Sarnthein, M., Lamy, F., and Tiedemann, R.: High-resolution

980   radiocarbon-based age records trace episodes of *Zoophycos* burrowing, Marine

981   Geology, 403, 48-56, http://doi:10.1016/j.margeo.2018.04.01, 2018.

982   Küssner, K., Sarnthein, M., Lamy, F., Michel, E., Mollenhauer, G., Siani G., and

983   Tiedemann, R.: Glacial-to-deglacial reservoir ages of surface waters in the southern

984   South Pacific. Paleoceanography and Paleoclimate, 54 ms-pp, 2020 subm.

985   Lascu, I., Feinberg, J.M., Dorale, J.A., Cheng, H., and Edwards, R.L.: Age of the

986   Laschamp excursion determined by U-Th dating of a spelothem geomagnetic record

987   from North America. Geology, 44, 139-142, doi:10.1130/G37490.1. 2016

988   Lindsay, C.M., Lehman, S.J., Marchitto, T.M., and Ortiz, J.D.: The surface
989   expression of radiocarbon anomalies near Baja California during deglaciation. Earth
990   Planetary Science Letters, 422, 67-74, 2015.

991   Lippold, J., Gutjahr, M., Blaser, P., Christner, E., de Cavalho-Fereira, M.L., Mulitza,
992   S. et al.: Deep-water provenance and dynamics of the (de)glacial Atlantic meridional
993   overturning circulation, Earth Planetary Science Letters, 445, 68-78, 2016.

994   Lisiecki, L.E. and Stern, J.V.: Regional and global benthic d^{18}O stacks for the last
995   glacial cycle. Paleoceanography, 31, doi:10.1002/2016PA003002, 2016.

996   Löwemark, L. and Grootes, P.M.: Large age differences between planktic
997   foraminifers caused by abundance variations and Zoophycos bioturbation,
998   Paleoceanography, 19, PA2001, doi:10.1029/2003PA000949, 2004.

999   Marcott, S.A., Bauska, T.K., Buizert, C., Steig, E.J., Rosen, J.L., Cuffey, K.M.,
1000   Fudge, T.J., Severinghaus, J.P., Ahn, J., Kalk, M.L., McConnell, J.R., Sowers, T.,
1001   Taylor, K.C., White, J.W.C., and Brook, E.J.: Centennial-scale changes in the global
1002   carbon cycle during the last deglaciation, Nature, 514, 616-619,
1003   doi:10.1038/nature13799, 2014.

1004   Marshall, M., Schlolaut, G., Brauer, A., Nakagawa, T., Staff, R.A., Bronk Ramsey,
1005   C., Lamb, H., Gotanda, K., Haraguchi, T., Yokoyama, Y., Yonenobu, H., Tada, R.,
1006   SG06 project members: A novel approach to varve counting using µXRF and X-
1007   radiography in combination with thin-section microscopy, applied to the Late Glacial
1008   chronology from Lake Suigetsu, Japan, Quaternary Geochronology 13, 70-80, 2012.

1009   McCave, I.N., Carter, I., and Hall, I.R.: Glacial-interglacial changes in water mass
1010   structure and flow in the SW Pacific Ocean, Quaternary Science Rev., 27, 1886–1908,
1011   2008.

1012   Matsumoto, K.: Radiocarbon-based circulation age of the world oceans, J. Geophys.
1013   Res.: Oceans 112(C9), C09004. https://doi.org/10.1029/2007JC004095, 2007.

1014   Menviel, L., Spence, P., Yu, J., Chamberlain, M.A., Matear, R.J., Meissner K.J., and
1015   England, M.H.: Southern Hemisphere westerlies as a driver of the early deglacial
1016   atmospheric CO2 rise, Nature communications, 9:2503, DOI:10.1038/s41467-018-
1017   04876-4, 2018.

1018   Millo, C., Sarnthein, M., and Erlenkeuser, M.: Variability of the Denmark Strait
1019   Overflow during the Last Glacial Maximum, Boreas, 35, 50-60, 2006.

1020   Muglia, J., Skinner, L., and Schmittner, A.: Weak overturning circulation and high
1021   Southern Ocean nutrient utilization maximized glacial ocean carbon, Earth and

Planetary Science Letters 496, 47-56, 2018.

Muschitiello, F., D'Andrea, W.J., Schmittner, A., Heaton, T.J., Balascio, N.L., deRoberts, N., Caffee, M.W., Woodruff, T.E., Welten, K.C., Skinner, L.C., Simon, M.H., and Dokken T.M.: Deep-water circulation changes lead North Atlantic climate during deglaciation, Nature Communications 10, 1272, doi.org/10.1038/s41467-019-09237-3, 2019.

Naughton, F., Costas, S., Gomes, S.D., Desprat, S., Rodrigues, T., Sanchez Goñi, M.F., Renssen, H., Trigo, R., Bronk-Ramsey, C., Oliveira, D., Salgueiro, E., Voelker, A.H.L., and Abrantes, F.: Coupled ocean and atmospheric changes during Greenland stadial 1 in southwestern Europe, Quaternary Science Reviews, 212, 108-120, 2019.

Nydal R., Lovseth K., and Skogseth F. H.: Transfer of bomb ^{14}C to the ocean surface, Radiocarbon 22(3), 626–635, 1980.

Okazaki, Y., Sagawa, T., Asahi, H., Horikawa, K., and Onodera, J.: Ventilation changes in the western North Pacific since the last glacial period, Climate of the Past, 8, 17-24, doi:10.5194/cp-8-17-2012, 2012.

Paillard, D., Labeyrie, L., and Yiou, P.: Macintosh program performs time-series analysis, *Eos Trans, AGU,* **77**: 379, 1996.

Rae, JW.B. and W. Broecker, W.: What fraction of the Pacific and Indian oceans' deep water is formed in the Southern Ocean? Biogeosciences, 15, 3779-3794, 2018.

Rae, J., Sarnthein, M., Foster, G., Ridgwell, A., Grootes, P.M., and Elliott T.: Deep water formation in the North Pacific and deglacial CO_2 rise*, Paleoceanography, 29, doi:10.1002/2013PA002570, 645–667, 2014.

Rafter, P.A., Herguera, J.-C., and Southon, J.R.: Extreme lowering of deglacial seawater radiocarbon recorded by both epifaunal and infaunal benthic foraminifera in a wood-dated sediment core, Climate of the Past 14, 1977–1989, 2018.

Reimer P.J., Bard, E., Bayliss, A., Beck, J. W., Blackwell, P.G., Bronk Ramsey, C., Buck, C.E., Cheng, H., Edwards, R.L., and Friedrich, M.: IntCal13 and Marine13 radiocarbon age calibration curves 0–50,000 years cal. BP, Radiocarbon 55, 1869–1887, 2013.

Reimer, P.J., et al.: The IntCal 20 northern hemisphere radiocarbon calibration curve (0-55 kcal BP), Radiocarbon, 2020 (in press).

Robinson, L.F., Adkins, J.F., Keigwin, L.D., et al..: Radiocarbon variability in the western North Atlantic during the last deglaciation, Science, 310, 1469-1473, 2005.

1055   Ronge, T. A., Tiedemann, R., Lamy, F., et al.: Radiocarbon constraints on the extent
1056   and evolution of the South Pacific glacial carbon pool, Nature Comm. 7:11487, 2016.

1057   Ronge, T.A., Sarnthein, M., Roberts, J., Lamy, F., and Tiedemann, R.: East Pacific
1058   Core PS75/059-2: Glacial-to-deglacial stratigraphy revisited, Paleoceanography and
1059   Paleoclimatology, 34 (4), 432-435, DOI:10.1029/2019PA003569, 2019.

1060   Sarnthein, M., Winn, K., Jung, S.J., Duplessy, J.C., Labeyrie, L., Erlenkeuser, H.,
1061   and Ganssen, G.: Changes in east Atlantic deepwater circulation over the last 30,000
1062   years: eight time slice reconstructions, Paleoceanography, 9(2), 209–267, 1994.

1063   Sarnthein, M., Pflaumann, U., and Weinelt, M.: Past extent of sea ice in the northern
1064   North Atlantic inferred from foraminiferal paleotemperature estimates,
1065   Paleoceanography, 18(2), 2003.

1066   Sarnthein, M., Grootes, P.M., Kennett, J.P., and Nadeau, M.: [14]C Reservoir ages
1067   show deglacial changes in ocean currents and carbon cycle, Geophys. Monograph –
1068   Am. Geophys. Union, 173, 175–196, 2007.

1069   Sarnthein, M., Grootes, P.M., Holbourn, A., Kuhnt, W., and Kühn, H.: Tropical
1070   warming in the Timor Sea led deglacial Antarctic warming and almost coeval
1071   atmospheric CO_2 rise by >500 yr, Earth Planetary Science Letters, 302, 337-348, 2011.

1072   Sarnthein, M., Schneider, B., and Grootes, P.M.: Peak glacial 14C ventilation ages
1073   suggest major draw-down of carbon into the abyssal ocean, Climate of the Past, 9 (1),
1074   925–965, 2013.

1075   Sarnthein, M., Balmer, S., Grootes, P.M., and Mudelsee, M.: Planktic and benthic
1076   14C reservoir ages for three ocean basins, calibrated by a suite of 14C plateaus in the
1077   glacial-to-deglacial Suigetsu atmospheric 14C record, Radiocarbon, 57, 129–151, 2015.

1078   Sarnthein, M. and Werner, K.: Early Holocene planktic foraminifers record species-
1079   specific ^{14}C reservoir ages in Arctic Gateway, Marine Micropaleontology, 135, 45-55.
1080   DOI:10.1016/j.marmicro.2017.07.002, 2018.

1081   Schlolaut, G.: A unique and easy-to-use-tool to deal with incompletely varved
1082   archives 782 – the Varve Interpolation Program 3.0.0, Quaternary Geochronology, 2019
1083   (in press).

1084   Schlolaut, G., Staff, R.A., Marshall, M.H., Brauer, A., Bronk Ramsey, C., Lamb, H.F.,
1085   and Nakagawa, T.: Microfacies analysis of the Lake Suigetsu (Japan) sediments from
1086   ~50 to ~10 ka BP and an extended and revised varve based chronology, Quaternary
1087   Science Reviews, 200, 351-366, 2018.

1088   Schmittner, A. and Lund, D.C.: Early deglacial Atlantic overturning decline and its
1089   role in atmospheric CO_2 rise inferred from carbon isotopes (δ^{13}C), Climate of the Past,
1090   11, 135-152, 2015.

1091   Schroeder, J., Holbourn, A., Küssner, K., and Kuhnt, W.: Hydrological variability in
1092   the southern Makassar Strait during the last glacial termination, Quaternary Science
1093   Reviews, 154, 143-156, 2016.

1094   Sessford, E.G., Jensen, M.F., Tisserand, A.A., Muschitiello, F., Dokken, T.,
1095   Nisancioglu, K.H., and Jansen, E.: Consistent fluctuations on intermediate water
1096   temperature off the coast off Greenland and Norway suring Dansgaard-Oeschger
1097   events, Quaternary Science Reviews, 223, 105887, 1-17, 2019.

1098   Sherriff-Tadano, S., Abe-Ouchi, A., Yoshimori, M., Oka, A., and Chan, W.-L.:
1099   (Influence of glacial ice sheets on the Atlantic meridional overturning circulation through
1100   surface wind change, Climate Dynamics, 50 (7-8), 2881–2903, 2017.

1101   Siani, G., Michel, E., De Pol-Holz, R., DeVries, T., Lamy, F., Carel, M., Isguder, G.,
1102   Dewilde, F., Lourantou, A.: Carbon isotope records reveal precise timing of enhanced
1103   Southern Ocean upwelling during the last deglaciation, Nature Communications, 4,
1104   2758, 2013.

1105   Sikes, E.L. and Guilderson, T.P.: Southwest Pacific Ocean surface reservoir ages
1106   since the last deglaciation: Circulation insights from multiple-core studies. Paleocean-
1107   ography, 31, 298–310, doi:10.1002/2015PA002855, 2016.

1108   Simstich, J., Sarnthein, M., and Erlenkeuser, H.: Paired δ^{18}O signals of
1109   *Neogloboquadrina pachyderma* (s) and *Turborotalita quinqueloba* show thermal
1110   stratification structure in Nordic Seas, Mar. Micropaleontol., 912, 1–19, 2003.

1111   Skinner, L.C., Fallon, S., Waelbroeck, C., Michel, E., and Barker, S.: Ventilation of
1112   the deep Southern Ocean and deglacial CO2 rise, Science, 328, 1147–1151, 2010.

1113   Skinner, L.C., Waelbroeck, C., Scrivner, A.E., and Fallon, S.J.:Radiocarbon
1114   evidence for alternating northern and southern sources of ventilation of the deep
1115   Atlantic carbon pool during the last deglaciation, PNAS, 111, 5480–5484, 2014.

1116   Skinner, L.C. *et al.*: Reduced ventilation and enhanced magnitude of the deep
1117   Pacific carbon pool during the last glacial period, Earth Planetary Science Letters*,* **411**,
1118   45-52, 2015.

1119   Skinner, L.C., Primeau, F., Freeman, E., de la Fuente, M., Goodwin, P.A.,
1120   Gottschalk, J., Huang, E., McCave, I.N., Noble, T.L., and Scrivner A.E.: Radiocarbon

1121 constraints on the glacial ocean circulation and its impact on atmospheric CO_2, Nature

1122 communications, 8:16010, DOI: 10.1038/ncomms16010, 2017.

1123   Skinner, L.C., Muschitiello, F., and Scrivner, A.E.: Marine reservoir age variability

1124 over the last deglaciation: Implications for marine carbon cycling and prospects for

1125 regional radiocarbon calibrations. Paleoceanography and Paleoclimate, 34,

1126 doi.org/10.1029/2019PA003667, 2019.

1127   Southon, J., Noronha, A.L., Cheng, H, Edwards, R.L., and Wang, Y.: A high-

1128 resolution record of atmospheric ^{14}C based on Hulu Cave speleothem H82, Quaternary

1129 Science Reviews, 33:32-41, 2012.

1130   Steffensen, J.P., Andersen, K.K., Bigler, M., et al.: High-Resolution Greenland Ice

1131 Core Data Show Abrupt Climate Change Happens in Few Years, Science, 321, 680;

1132 DOI: 10.1126/science.1157707, 2008.

1133   Stern, J.V. and Lisiecki, L.E.: North Atlantic circulaton and reservoir age changes

1134 over the past 41,000 years, Geophysical Research Letters, 40, 3693-3697,

1135 doi:10.1002/grl.5067, 2013.

1136   Stocker, T. and Johnsen, S.J.: A minimum thermodynamic model for the bipolar

1137 seesaw, Paleoceanography, 18 (4), 1087, doi:10.1029/2003PA000920, 2003.

1138   Stuiver, M. and Braziunas, T.V.: Modeling atmospheric ^{14}C influences and ^{14}C ages

1139 of marine samples to 10,000 B.C., Radiocarbon, 35, 137–189, 1993.

1140   Svensson, A., Andersen, K.K., Bigler, M., Clausen, H.B., Dahl-Jensen, D., Davies,

1141 S.M., Johnsen, S.J., Muscheler, R., Parrenin, F., Rasmussen, S.O., Röthlisberger, R.,

1142 Seierstad, I., Steffensen, J.P., and Vinther, B.M.: A 60 000 year Greenland stratigraphic

1143 ice core chronology, Climate of the Past, 4, 47–57, 2008.

1144   Toggweiler, J.R., Druffel, E.R.M., Key, R.M., and Galbraith, E.D.: Upwelling in the

1145 ocean basins north of the ACC. Part 2: How cool Subantarctic water reaches the

1146 surface in the tropics, J. Geophysical Research, DOI:10.1029/2018JC014795, 2019 (in

1147 press).

1148   Turney, C.S.M., Fifield, L.K., Hogg, A.G., et al.: Using New Zealand kauri (*Agathis

1149 australis*) to test the synchronicity of abrupt climate change during the Last Glacial

1150 Interval (60,000–11,700 years ago), Quatern. Sci. Rev., 29, 3677–3682, 2010.

1151   Turney, C.S.M., Jones, R.T., Phipps, S.J., et al.: Rapid global ocean-atmosphere

1152 response to Southern Ocean freshening during the last glacial, Nature communications,

1153 8:520, doi:10.1038/s41467-017-00577-6, 2017.

1154   Umling, N.E. and Thunnell, R.C.: Synchronous deglacial thermocline and deep-

1155   water ventilation in the eastern equatorial Pacific, Nature communications, 8, 14203.

1156   DOI: 10.1038/ncomms14203, 2017.

1157   Waelbroeck, C., Duplessy, J.-C., Michel, E., Labeyrie, L., Paillard, D., and Duprat, J.:

1158   The timing of the last deglaciation in North Atlantic climate records, Nature, 412, 724–

1159   727, 2001.

1160   Waelbroeck, C., Skinner, L.C., Labeyrie, L., Duplessy, J.-C., Michel, E., Riveiros,

1161   N.V., Gherardi, J.-M., and Dewilde, F.: The timing of deglacial circulation changes in the

1162   Atlantic, Paleoceanography, 26, PA3213, https://doi.org/10.1029/2010PA002007, 2011.

1163   Wallmann, K., Schneider, B., and Sarnthein, M.: Effects of eustatic sea-level

1164   change, ocean dynamics, and nutrient utilization on atmospheric pCO_2 and seawater

1165   composition over the last 130,000 years – a model study, Climate of the Past, 12, 339-

1166   375, doi: 10.5194/cp-12-339-2016, 2016.

1167   Wang Y.C, Cheng, H., Edwards, R.L., An, Z.S., Wu, J.Y., Shen, C.-C., and Dorale,

1168   J.A.: A high-resolution absolute-dated Late Pleistocene monsoon record from Hulu

1169   Cave, China, Science, 294, 2345-2348. DOI: 10.1126/science.1064618, 2001.

1170   Wang, L.J., Sarnthein, M., Erlenkeuser, H., Grimalt, J., Grootes, P., Heilig, S.,

1171   Ivanova, E., Kienast, M., Pelejero, C., and Pflaumann, U.: East Asian monsoon climate

1172   during the late Pleistocene: High-resolution sediment records from the South China

1173   Sea, Marine Geology, 156, 245-284, 1999.

1174   Wang, P., Clemens, S., Beaufort, L., Braconnot, P., Ganssen, G., Jian, Z., Kershaw,

1175   P., and Sarnthein, M.: SCOR/IMAGES Working Group 113 SEAMONS: Evolution and

1176   variability of the Asian Monsoon System: State of the art and outstanding issues,

1177   Quaternary Science Reviews, 24 (5-6), 595-629, 2005.

1178   WAIS Divide Project Members: Onset of deglacial warming in West Antarctica driven

1179   by local orbital forcing. Nature, 500, 440-444. doi:10.1038/nature12376, 2013.

1180   Xu, J., Kuhnt, W., Holbourn, A., Regenberg, M., and Andersen, N.: Indo-Pacific

1181   Warm Pool variability during the Holocene and Last Glacial Maximum, Paleoceanogr.,

1182   25, 16, 2010.

1183   Yamamoto, A., Abe-Ouchi, A., Ohgaito, R., Ito, A., and Oka, A.: Glacial CO_2

1184   decrease and deep-water deoxygenation by iron fertilization from glaciogenic dust,

1185   Climate of the Past, 15, 981-996.

1186   Yashayaev, I., Seidov, D., and Demirov, E.: A new collective view of oceanography

1187   of the Arctic and North Atlantic basins, Progress in Oceanography, 132, 21 pp.,

1188   DOI:http://dx.doi.org/10.1016/j.pocean.2014.12.012, 2015.

1189   Zhao, N. and Keigwin, L.D.: An atmospheric chronology for the glacial-deglacial

1190   Eastern Equatorial Pacific, Nature communications, 9:3077, DOI:10.1038/s41467-018-

1191   05574-x, 2018.

1192   Zhao, N., Marchal, O., Keigwin, L., Amrhein, D., and Gebbie, G.: A synthesis of

1193   deep-sea radiocarbon records and their (in) consistency with modern ocean ventilation,

1194   Paleoceanography and Paleoclimatology, 33, 128-151, 2018.

1195 TABLE CAPTIONS

1196

1197 ⅄ **Table 1 a and b.** Summary of varve- and U/Th model-based age estimates (Schlolaut

1198 et al., 2018; Bronk Ramsey et al., 2012) for ~30 plateau (pl.) boundaries in the

1199 atmospheric ^{14}C record identified in Lake Suigetsu Core SG06$_{2012}$ by means of visual

1200 inspection over the interval 10.5–27 cal. ka (Sarnthein et al., 2015, suppl. and modified).

1201 At the right hand side, three columns give the average (Ø) and uncertainty range of ^{14}C

1202 ages for each ^{14}C plateau.

SUIGETSU SG06_2012 Plateau no.	Plateau Top Varve-based age (yr BP)	U/Th-based age (yr BP)	Depth (cm c.d.)	Plateau Base Varve-based age (yr BP)	U/Th-based age (yr BP)	Depth (cm c.d.)	Ø 14C Age of 14C Plateau (14C yr)	±Uncertainty (14C yr)	14C age BP min/max. (1.6 σ range)
'Preboreal'	10525	10560	1325	11100	11108	1383	9525	−170/+110	9356/ 9635
'Top YD'	11290	11281	1402	11760	11755	1453	10060	−100/+35	9963/ 10095
'YD'	11950	11895	1467	12490	12475	1525	10380	−170/ 124	10211/ 10504
'no name'	12885	12780	1555	13160	13080	1582	11000	−85/ 114	10915/ 11114
1a	13580	13656	1626	13980	14042	1657	12006	100	11857/ 12050
1	14095	14160	1666	15095	15100	1740	12471	185	12315/ 12683
2a	15310	15420	1754	16140	16520	1802	13406	245	13174/ 13665
2b	16075	16520	1802	16400	16930	1820	13850	40	13808/ 13885
3	16835	17500	1847	17500	18220	1888	14671	105	14582/ 14792
4	17880	18650	1913	18830	19590	1971	15851	190	15661/ 16044

1203

5a	18960	*19720*	1978	19305	*20240*	2003	**16670**	90	16570/16750
5b	19305	*20240*	2003	20000	*20900*	2032	**17007**	190	16830/17247
6a	20190	*21000*	2050	20920	*21890*	2105	**17667**	262	17435/17960
6b	20920	*21890*	2105	21275	*22300*	2132	**18075**	140	17960/18240
7	21375	*22400*	2140	21790	*22870*	2171	**18843**	117	18741/18975
8	21835	*22940*	2175	22730	*24250*	2257	**19715**	−290 325	19425/20041
9	22730	*24250*	2257	23395	*25150*	2312	**20465**	−227 263	20238/20728
10a	23935	*25880*	2358	25080	*27000*	2400	**22328**	−380 270	21946/22600
10b	25080	*27000*	2400	25800	*27600*	2426	**22708**	−475 440	22233/23147
11	26110	*27770*	2443	27265	*28730*	2525	**24088**	−360 505	23727/24595

1204

1205

1206 ⊻ **Table 2**. Temporal match of various ^{14}C plateaus with deglacial periods of major

1207 atmospheric CO_2 rise and ocean warmings (AA = Antarctic; GIS = Greenland

1208 Interstadial).

pCO$_2$ RISE (~12 ppm)	Plateau no.	Plateau boundaries
AGE based on annual layers AA ice core (Marcott et al. 2014)		AGE range (cal. ka) based on **U/Th model ages** (Bronk Ramsey et al., 2012)
11.7 – 11.5	# 'Top YD'	**11.83 – 11.3**
14.8 – 14.53	# 1	**15.1 – 14.2**
16.4 – 16.15	# 2a	**16.52 – 15.5**
17.4 – ~17.1	(data gap)	**17.3 – 17.1**

FURTHER POTENTIAL CORRELATIVES:

Progressive N. Atlantic warming during the YD at 12.39 – 12.03 ka *	# 'YD'	**12.46 – 11.98**
Onset of Antarctic ** warming at 18.3–17.6 ka (ice-based time scale)	#3	**18.22 – 17.5**
Onset of North Atlantic *** warming at 19.3–18.6 ka (U/Th-based time scale)	# 4	**19.6 – 18.65**
Top H2: GIS 2 N. Atlantic warming at 23.4 – 23.3 ka ****	#8	**24.25 – 22.95**

AGE CONTROL based on

* Naughton et al. (2019), ** Kawamura et al. (2007),

*** Balmer and Sarnthein (2018), **** Grootes and Stuiver (1997)

1209

1210 ¥ **Table 3** a-c. [14]C reservoir / ventilation ages of surface (top 50-100 m) and bottom

1211 waters vs. U/Th-based model age at 19/22 core sites in the ocean. (a) Spatial and

1212 temporal changes over early and late LGM (24–21 and 21–18.7 cal. ka), (b) HS-1, and

1213 the B/A. Late LGM estimates (average res. age of Plateau 4-5) are compared to model-

1214 based estimates of Muglia et al. (2018). (c) Data sources. For core locations see Fig. 7.

1215 (a)

Sediment Core U/Th-based model age Plateau (Pl.) no.	Latitude	Longitude	Water depth (m)	LGM pla. res. age 24–21 ka (early LGM) Pl. 8 - 7 - 6	Error (yr)	21–18.7 ka (late LGM) Pl. 5 - 4	Error (yr)	LGM model res. age strong AMOC (yr)	res. age weak (yr)
ATLANTIC O.									
PS2644	67°52.02'N	21°45.92'W	777	2100	±390	1920–2200	±325 –±12!	1136	1100
GIK 23074	66°66.67'N	4°90'E	1157	620–790	±145–±270	550–1175	±100–±200	1054	1059
MD08-3180	38°N	31°13.45'W	3064	–		320–605	±125–±405	827	887
SHAK06-5K	37°34'N	10°09'W	2646	675–800		500–660		872	855
(= MD99-2334)	(37°48'N	10°10'W	3146						
ODP 1002	10°42.37'N	65°10.18'W	893	700–210	±230–±310	25 – -205	±205–±215	751	738
GeoB 3910-1	4°15'S	36°21'W	2361	–		–		779	796
GeoB 1711-4	23°17'S	12°23'W	1976	1080	±290	730–840	±240–±190	711	721
KNR 159-5-36GGC	27°31'S	46°48'W	1268	540	±140	870	±120	757	777
MD07-3076	44°4'S	4°12'W	3770	–		2300	±200	928	989
INDIAN O./TIMOR SEA									
MD01-2378	13°08.25'S	121°78.8'E	1783	–		2000–1700	±300–±320	885	890
PACIFIC O.									
MD02-2489	54°39.07'N	148°92.13'W	3640	–		1560–1110	±310–±335	972	965
MD01-2416	51°26.8'N	167°72.5'E	2317	–		1710	±440	1227	1202
ODP 893A	34°17.25'N	120°02.33'W	588	–		1065	±280	839	846
MD02-2503	34°16.6'N	120°01.6'W	580	–		–		839	846
GIK 17940	20°07.0'N	117°23.0'E	1727	1820–1260	±320–±230	hiatus		836	838
(= SO50-37)	18°55'N	115°55'E	2655	1820–1260				836	840
PS75/104-1	44°46'S	174°31'E,	835	1650–1280	±210-±320	1500	±340	881	895
(= SO213-84)	45°7.5'S	174°34,9'E	972	1650–1280	±210-±320	1500	±340	881	895
MD07-3088	46°S	75°W	1536	385	±315	380-450	±140–±230	917	–
SO213-76-2	46°13'S	178°1.7´W	4339	–		1460–990	±340–±550	915	842
PS97/137-1	52°39.5'S	75°33.9'E	1027	600–1180	±465	1180–800	±90–±225	1505	1419

1216

1217 (b)

Sediment Core U/Th-based model age Plateau (Pl.) no.	HS-1 pla. res. age 18 –16.5 ka Pl. 3 - 2b (yr)	Error (yr)	16.5–15.5 ka Pl. 2a (yr)	Error (yr)	B/A pla. res. age 14.7 –13.6 ka Pl. 1 - 1a	Error (yr)	LGM be. vent age (yr) early	late	LGM b.w. model age strong AMOC (yr)	weak (yr)
ATLANTIC O.										
PS2644	1775–1660	±105–±160	1900	±355	–		345	2400	948	918
GIK 23074	1730–2000	±125–±160	670	±310	140–310	±250–±100	375	375	960	931
MD08-3180	1420–1610	±310–±160	1460	±390	630–360	±310	600	600	1031	1004
SHAK06-5K	330–410		535		780–925		—	—	—	—
(= MD99-2334)							2200–2700	1900	—	—
ODP 1002	–100 – 20	±140	90	±345	355	±200	—		1247	1175
GeoB 3910-1	630–560	±160–±180	175	±475	210–230	±220–±110	2150	2150	—	—
GeoB 1711-4	660–690	±195–±45	420	±320	880	±255	1500	1500	1387	1714
KNR 159-5-36GGC	460–340	±380–±300	170	±700	180–230	±370–±310	1470	1470	1354	1563
MD07-3076	1650	±180	–		920	±230	3640	3640	1653	2060
INDIAN O./TIMOR SEA										
MD01-2378	740	±125	–		200–185	±345–±135	2720	—	1679	1881
PACIFIC O.										
MD02-2489	800–550	±155–±120	550	±305	440	±285		2625	2332	2595
MD01-2416	1480–1140	±135–±195	–		720–570	±285–±140		3700/5100	2400	2683
ODP 893A	1065–1490	±280–±125	1400	±370	520	±185		1430	1677	1705
MD02-2503	965–1365	±160–±165	1215	±325	395–535	±240–±130	—		—	—
GIK 17940	1210–1370	±200–±470	1045	±320	870–970	±325–±100	3300–1800		1807	1897
(= SO50-37)							3225	3225	2373	2667
PS75/104-1	1050	±265	1180	±350	800	±280	—	—	—	—
(= SO213-84)							1500	2400	1101	1146
MD07-3088	800–1090	±85–±125	1060	±275	1310–730	±125–±190	1360 ?	1600	1808	1701
SO213-76-2	840	±310	–		–			3460	1712	2001
PS97/137-1	1500–670	±90–±180	455	±270	–		1400–2400	2400/2900	1631	1871

1218

1219 (c)

Sediment Core	DATA Source	
ATLANTIC O.		
PS2644	Sarnthein et al. 2015	Be.data suppl.
GIK 23074	Sarnthein et al. 2015	Be.data suppl.
MD08-3180	Balmer et al. 2018	
SHAK06-5K	Ausin et al., 2020 subm.	
(= MD99-2334)	Skinner et al. 2014	
ODP 1002	Sarnthein et al. 2015	
GeoB 3910-1	Balmer et al. 2016	
GeoB 1711-4	Balmer et al. 2016	
KNR 159-5-36GGC	Balmer et al. 2016	data suppl.
MD07-3076	Balmer et al. 2016	
INDIAN O./TIMOR SEA		
MD01-2378	Sarnthein et al. 2015	
PACIFIC O.		
MD02-2489	Sarnthein et al. 2015	
MD01-2416	Sarnthein et al. 2015	modified
ODP 893A	Sarnthein et al. 2015	data suppl.
MD02-2503	Sarnthein et al. 2015	
GIK 17940	Sarnthein et al. 2015	
(= SO50-37)	Sarnthein et al. 2015	
PS75/104-1	Küssner et al., 2018+2020	
(= SO213-84)	Ronge et al., 2016	
MD07-3088	Küssner et al.,2020 subm	Siani et al. 2013
SO213-76-2	Küssner et al.,2020 subm	Ronge et al.2016
PS97/137-1	Küssner et al.,2020 subm	data suppl.

1220 (c)

1221 FIGURE CAPTIONS

1222

1223 – Fig. 1. Atmospheric ^{14}C ages of Lake Suigetsu plant macrofossils 10–20 cal. ka

1224 (bottom panel) and 19–29 cal. ka (top panel) vs. U/Th-based model age (blue dots;

1225 Bronk Ramsey et al., 2012). The 1:1 line reflects gradient of one ^{14}C yr / cal. yr. Double

1226 and triple ^{14}C measurements are averaged. (In part large) error bars of single ^{14}C ages

1227 are given in Suppl. Fig. S1. Suite of labeled horizontal boxes that envelop scatter bands

1228 of largely constant ^{14}C ages shows ^{14}C plateaus longer than 250 yr (plateau boundary

1229 ages listed in Table 1). Red and brown dots (powder samples from trench and wall) and

1230 + signs (off-axis samples) depict raw ^{14}C ages of Hulu stalagmites H82 and MSD

1231 (Cheng et al., 2018; Southon et al., 2012; plot offset by +3000 ^{14}C yr). Suite of short ^{14}C

1232 plateaus (black boxes) tentatively assigned to Hulu-based record occupies age ranges

1233 slightly different from those deduced for Suigetsu-based plateaus. The difference

1234 possibly results from short-term changes in the Old / Dead Carbon Fraction (ocf / dcf)

1235 that in turn may reflect major short-term changes in LGM and deglacial monsoon

1236 climate (Wang et al., 2001; Kong et al., 2005).
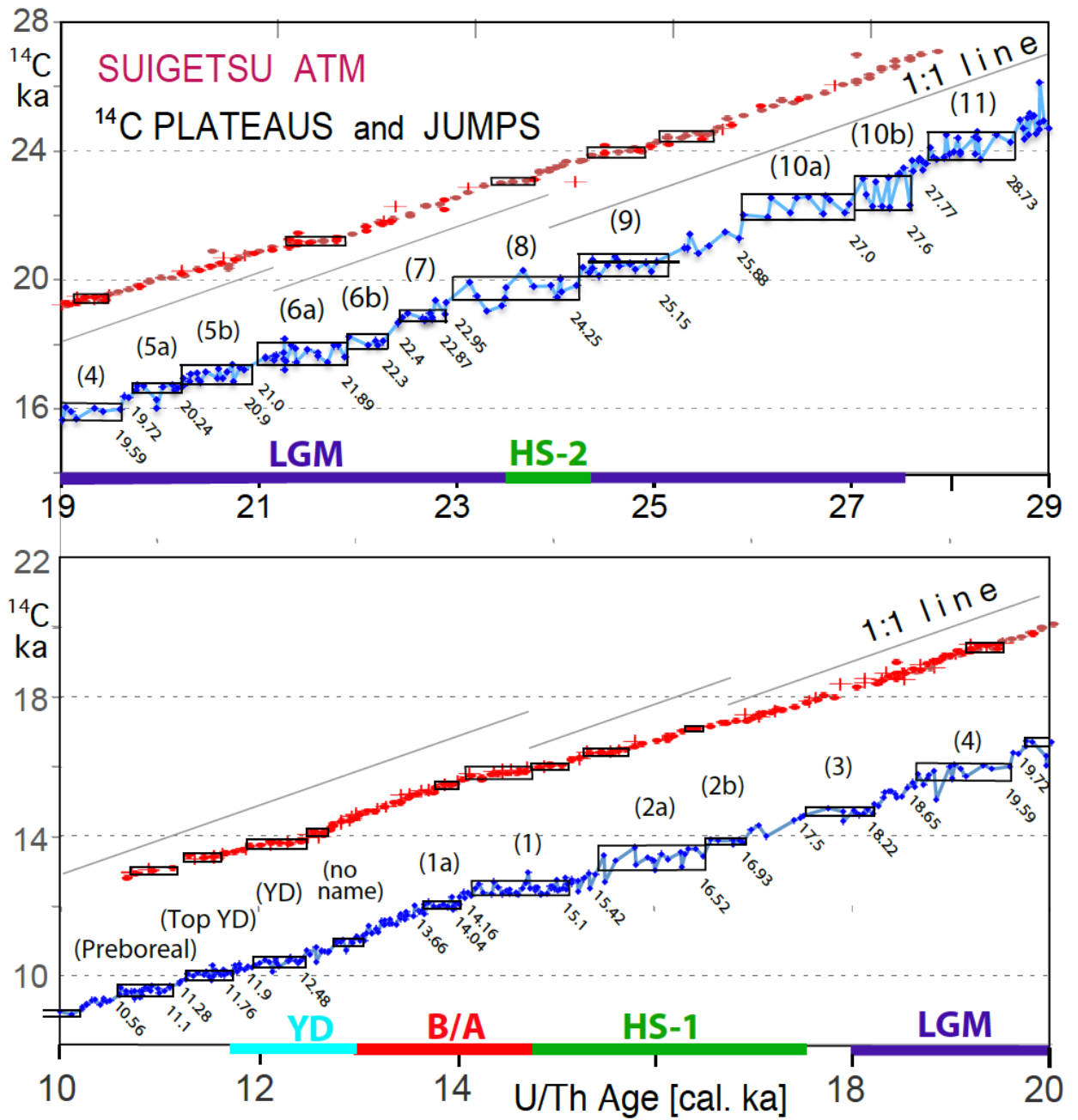
1237

1238

1239

1240   ⊻ Fig. 2. High-resolution record of atmospheric ¹⁴C jumps and plateaus (= suite of

1241   labeled horizontal boxes that envelop scatter bands of largely constant ¹⁴C ages

1242   extending over >300 cal. yr) in a sediment section of Lake Suigetsu vs. tree ring-based

1243   ¹⁴C jumps and plateaus 10–14.5 cal. ka (Reimer et al., 2013). Blue line averages paired

1244   double and triple ¹⁴C ages of Suigetsu plant macrofossils. Age control points (cal. ka)

1245   follow varve counts (Schlolaut et al., 2018) and U/Th model-based ages of Bronk

1246   Ramsey et al. (2012). YD = Younger Dryas, B/A = Bølling-Allerød.

1247
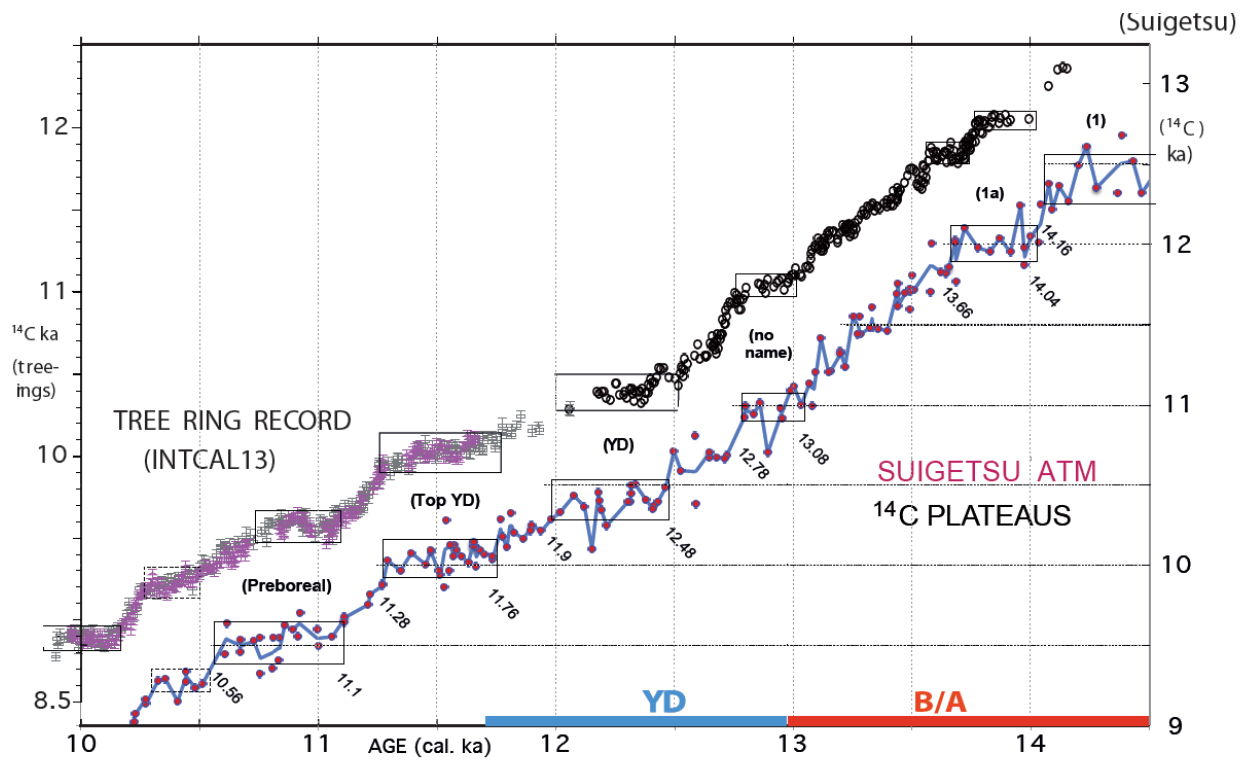
1248

1249

1250
1251
1252
1253
1254
1255
1256
1257
1258

1259 ∀ Fig. 3. Difference between Hulu Cave U/Th-based model ages (Southon et al., 2012;

1260 Bronk Ramsey et al., 2012; Cheng et al., 2018) and varve count-based cal. ages for

1261 atmospheric ^{14}C plateau boundaries in Lake Suigetsu sediment record (Schlolaut et al.,

1262 2018) (Sarnthein et al., 2015, suppl. and revised), displayed on the U/Th-based time

1263 scale 13–27 cal. ka.

1264
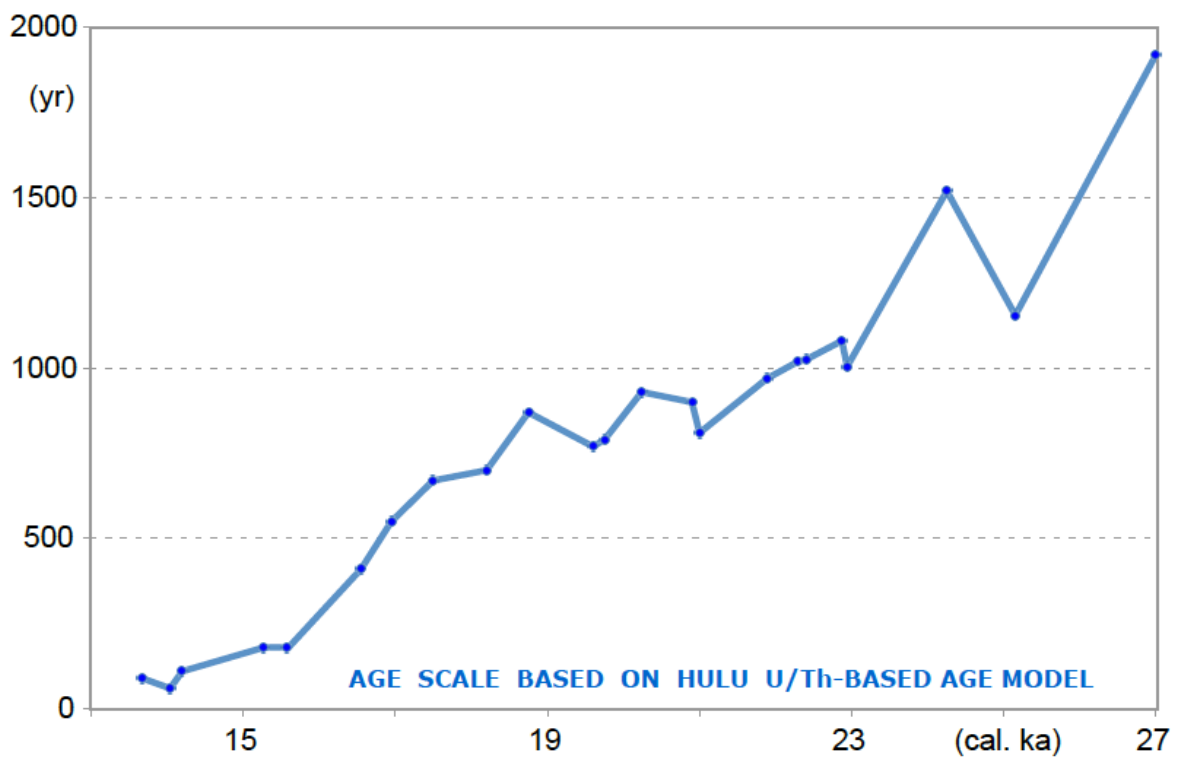
1265

1266

1267

1268

1269

1270

1271

1272

1273

1274 ⊻ Fig. 4 a and b. Atmospheric ^{14}C ages and plateaus (horizontal boxes) deduced from

1275 ^{10}Be production rates vs. GICC05 age scale (Adolphi et al., 2018) compared to the

1276 Suigetsu record of atmospheric ^{14}C plateaus vs. Hulu U/Th-based model ages (Southon

1277 et al., 2012; Cheng et al., 2018) for the intervals a) 10-20 and b) 19-29 cal ka BP.

1278
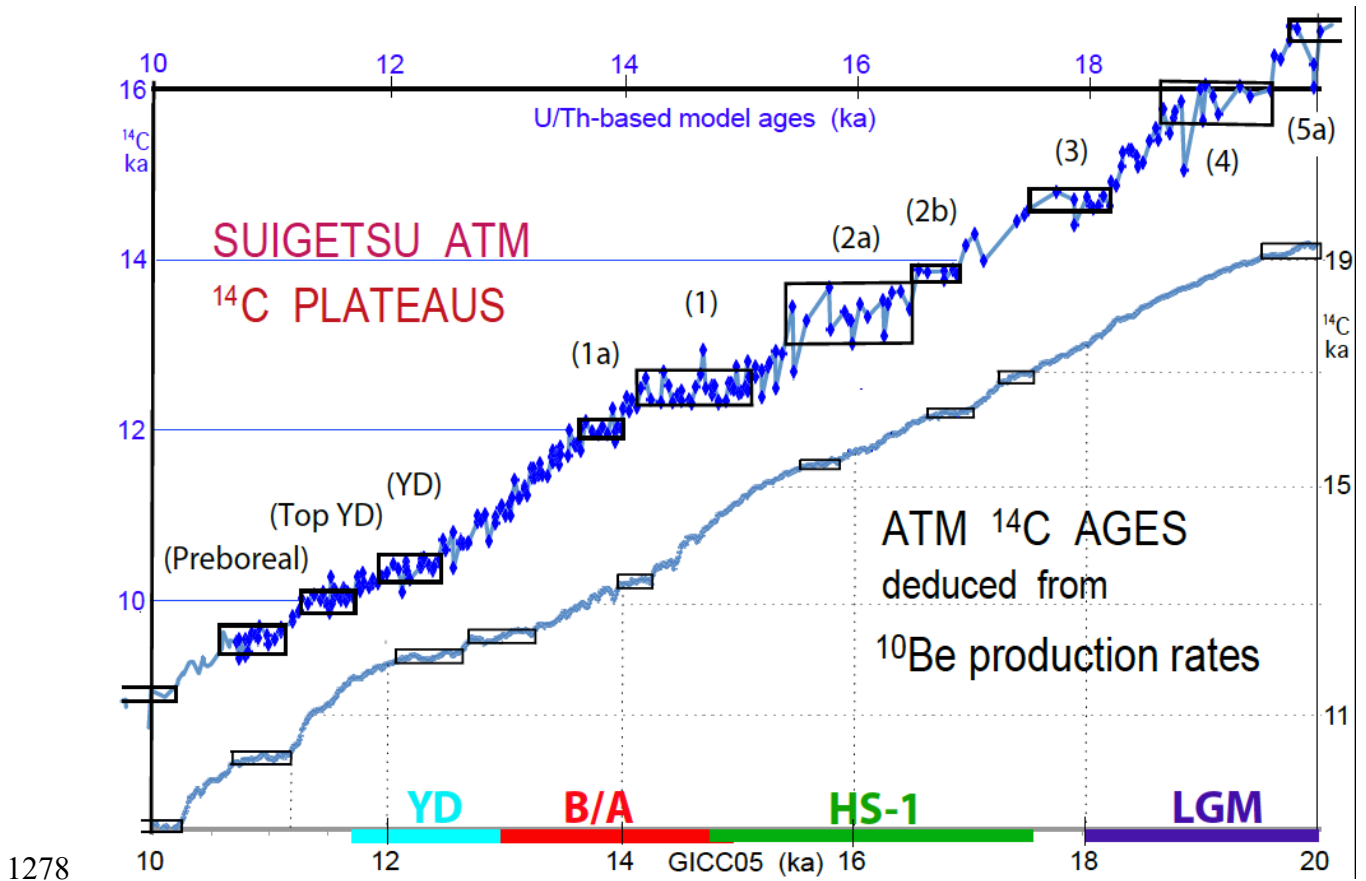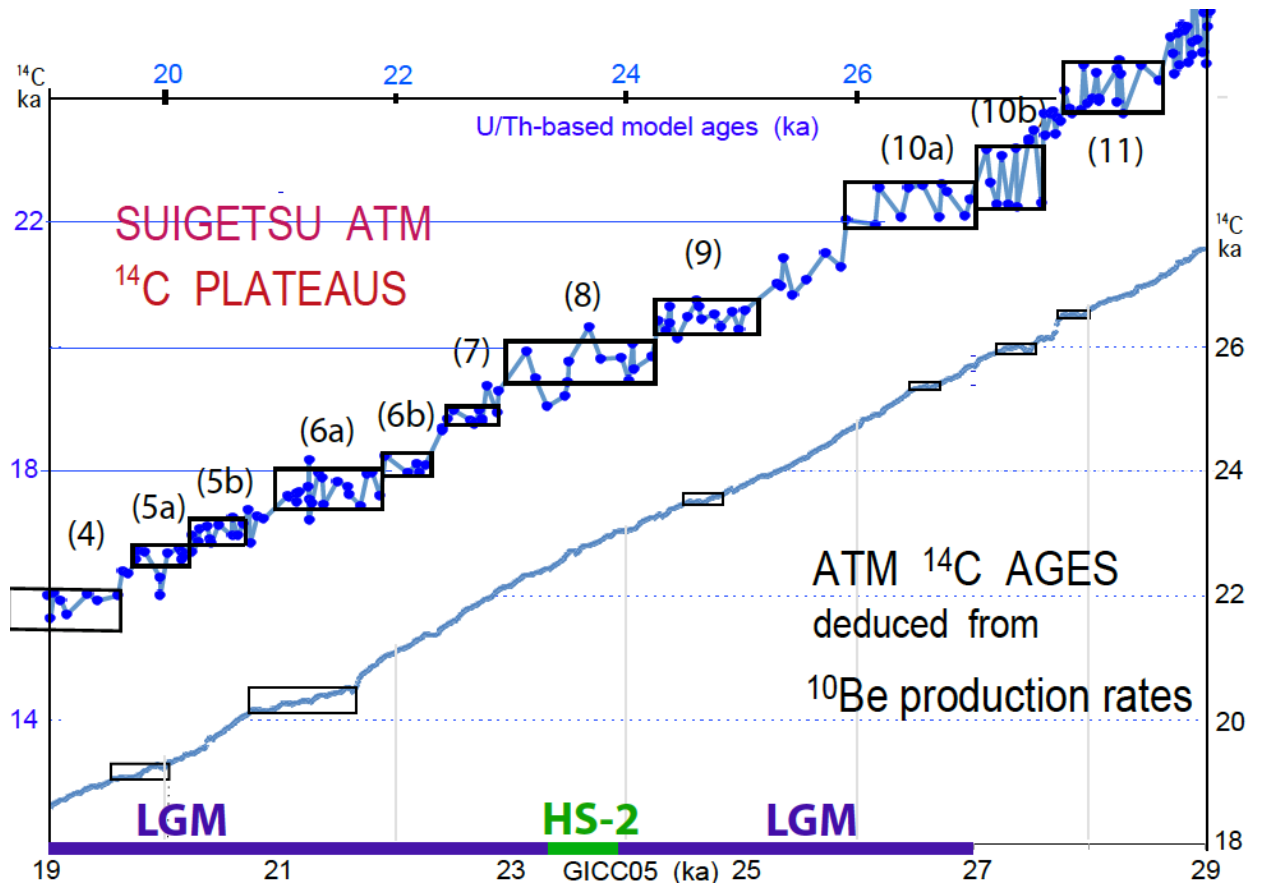
1279
1280
1281
1282
1283
1284
1285
1286
1287
1288
1289
1290
1291
1292

1293 ℽ Fig. 5. Sediment facies and microfacies zones in Lake Suigetsu Core SG06, ~13–32

1294 m depth (simplified and suppl. from Schlolaut et al., 2018). Microscopy-based frequency

1295 of siderite layers with quality level 1–3 (= running average of layer counts per 20 cm

1296 thick sediment section) serves as measure of seasonal lamination quality and shows

1297 gradual transitions between varved and poorly varved sediment sections. Rounded

1298 varve ages are microscopy based and constrain age of major facies and microfacies

1299 boundaries. ANI I to ANI III mark core sections with ultrafine lamination due to

1300 sedimentation rate minima, AT marks tephra layer named AT, 'Event layers' label major

1301 thin mud slides probably earth quake-induced.s
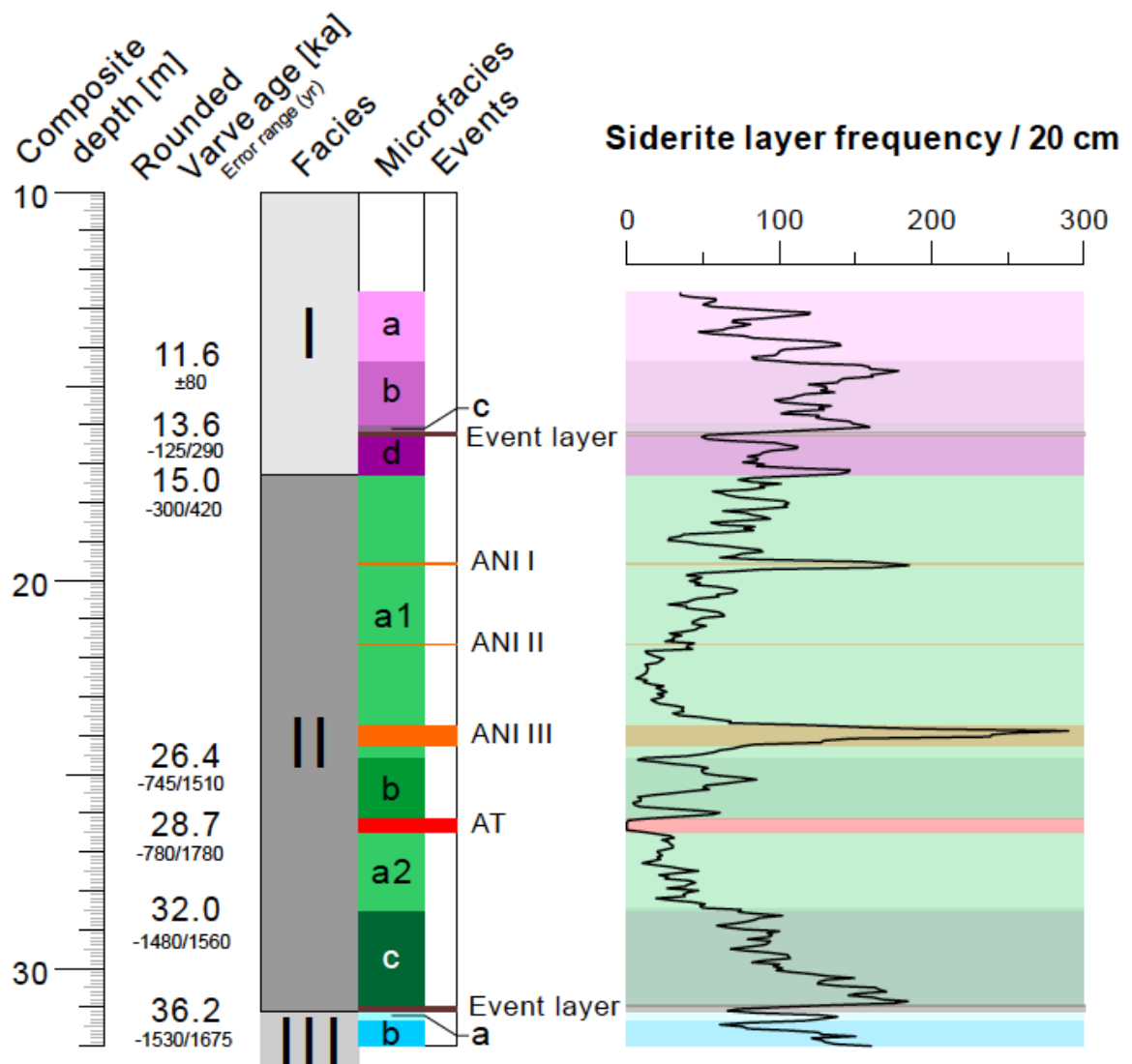
1302

1303 Fig. 6 (a). Four sudden steps (pink bars) in the deglacial atmospheric CO_2 rise at

1304   West Antarctic Ice Sheet Divide ice core (WDC) reflect events of fast ocean degassing,

1305   that may have contributed to the origin of deglacial ^{14}C plateaus. Age control based on

1306   ice cores (Marcott et al., 2014). (b) The steps are compared to suite of atmospheric [14]C

1307   plateaus dated by Hulu U/Th-based model ages (Bronk Ramsey et al., 2012). Hol =

1308   Holocene; YD = Younger Dryas; B/A = Bølling-Allerød; HS = Heinrich stadials 1 and 2;

1309   LGM = Last Glacial Maximum, GIS-2 = Greenland interstadial 2.

1310
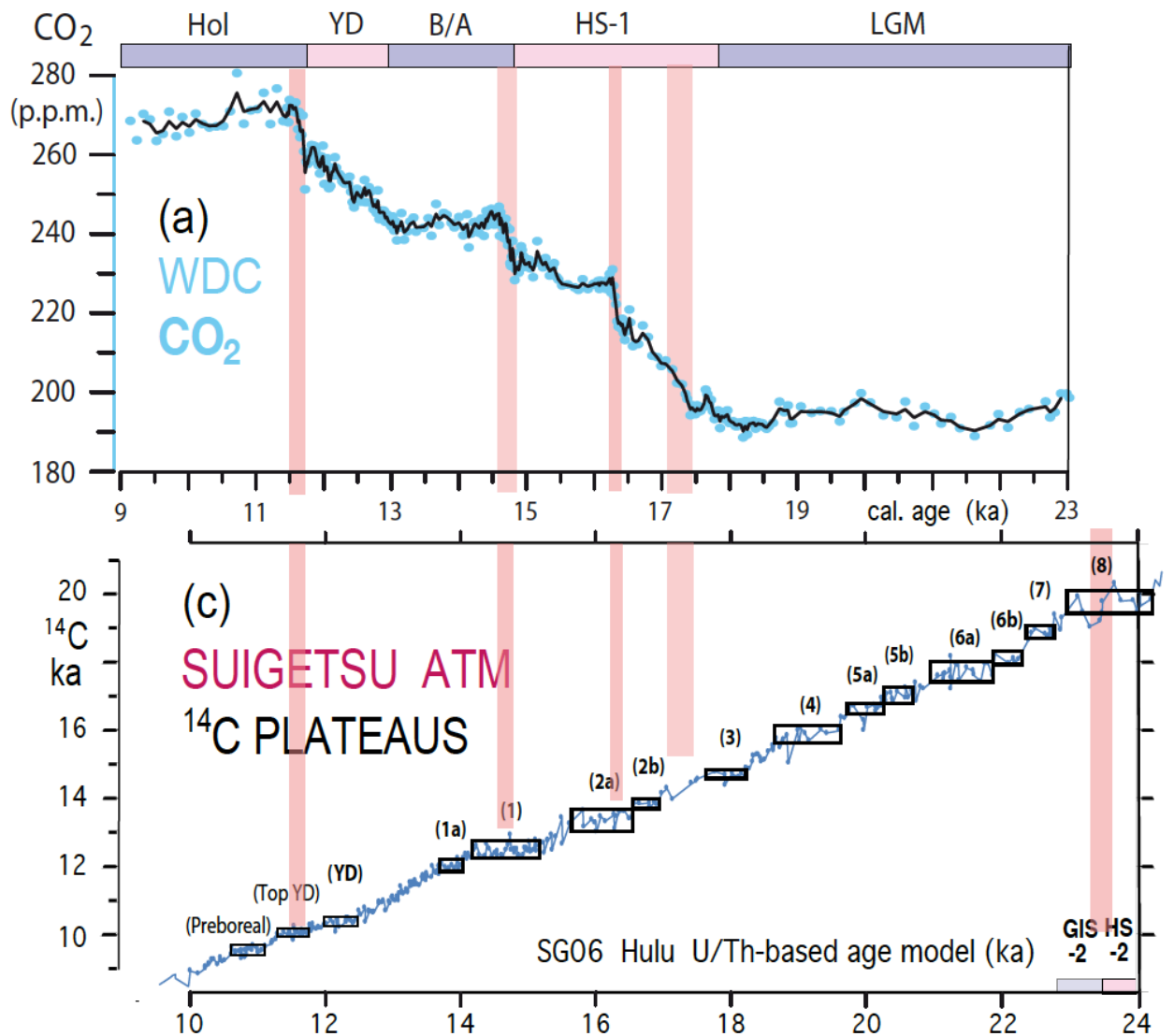
1311

1312

1313 ⊻ Fig. 7. Location (a) and water depth (km) (b) of sediment cores with age control based

1314 on ¹⁴C plateau tuning. ¹⁴C reservoir ages of cores labeled with 'w' are derived from

1315 samples with paired wood chunks and planktic foraminifers.
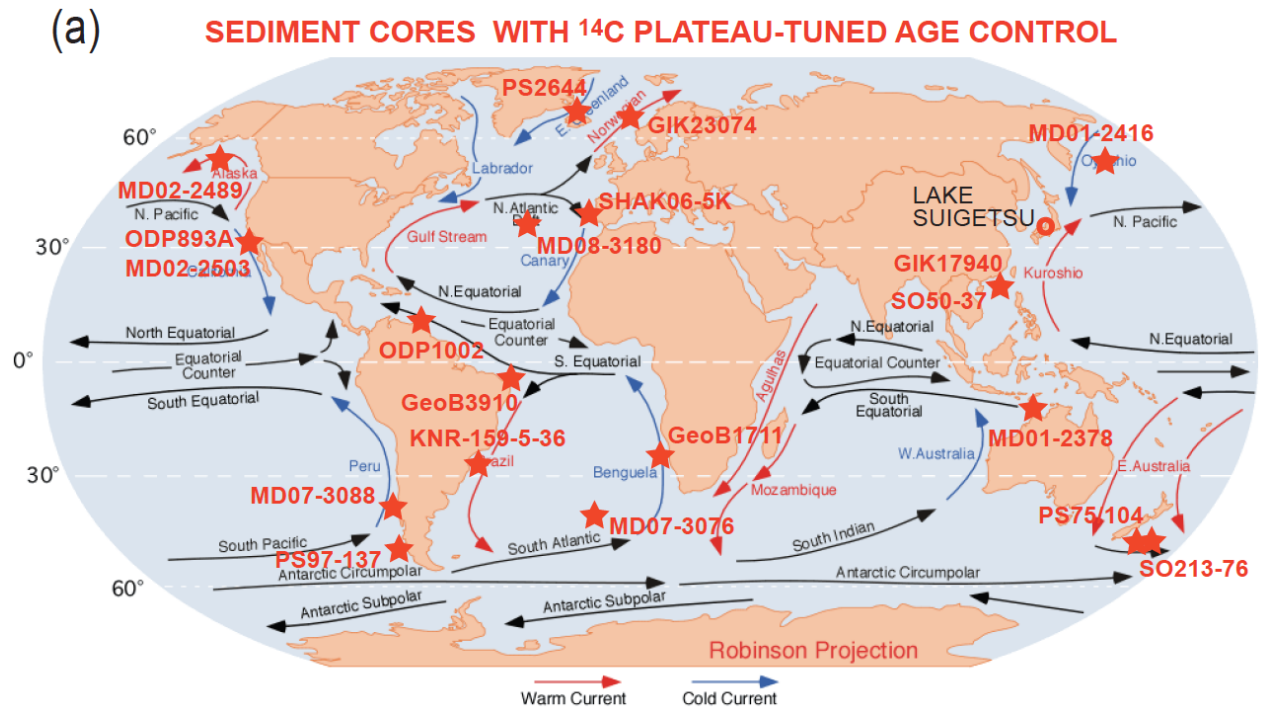
1316
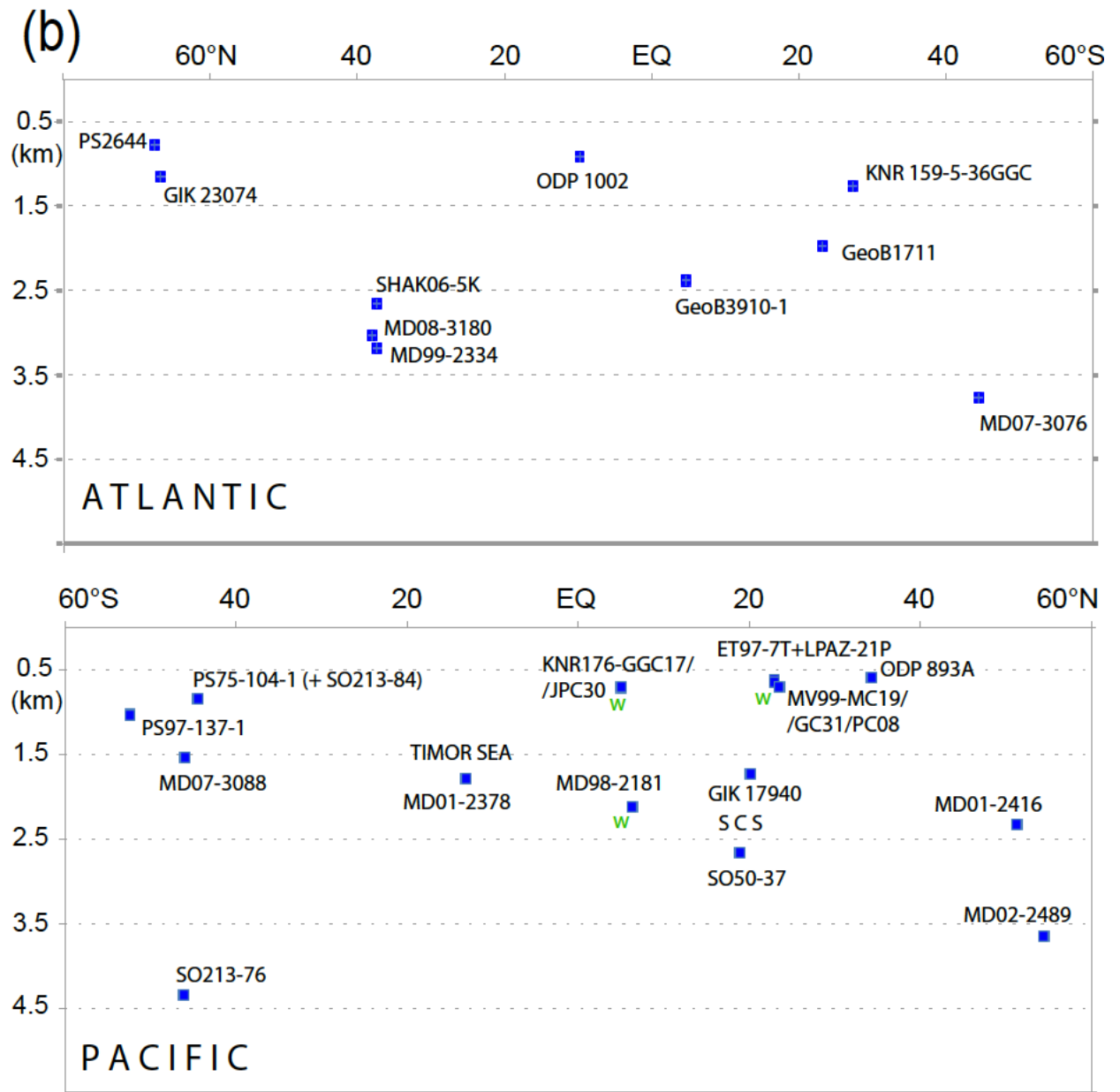
1317

1318

1319 ↯ Fig. 8. Global distribution of ^{14}C reservoir ages of Late LGM surface waters estimated

1320 (a) by means of ^{14}C plateau tuning of planktic 14C records. (b) Model-based estimates

1321 (GCM of Muglia et al., 2018, assuming an AMOC strength of 13 Sv) for sites with

1322 planktic foraminifera-based age values. X-Y graph (c) and map (d) show (rounded)

1323 differences between observed and modeled values and their intra-LGM trends. Minor

1324 differences are displayed in magenta, larger differences of >400 yr in red. Planktic

1325 habitat depths and model estimates are largely confined to 0–100 m water depth.

1326   Arrows of surface currents delineate different sea regions important to assess potential

1327   limits of spatial extrapolation of reservoir ages. Distribution of core numbers and

1328   references for ^{14}C records are given in Table 3a-c and Fig. 7a.
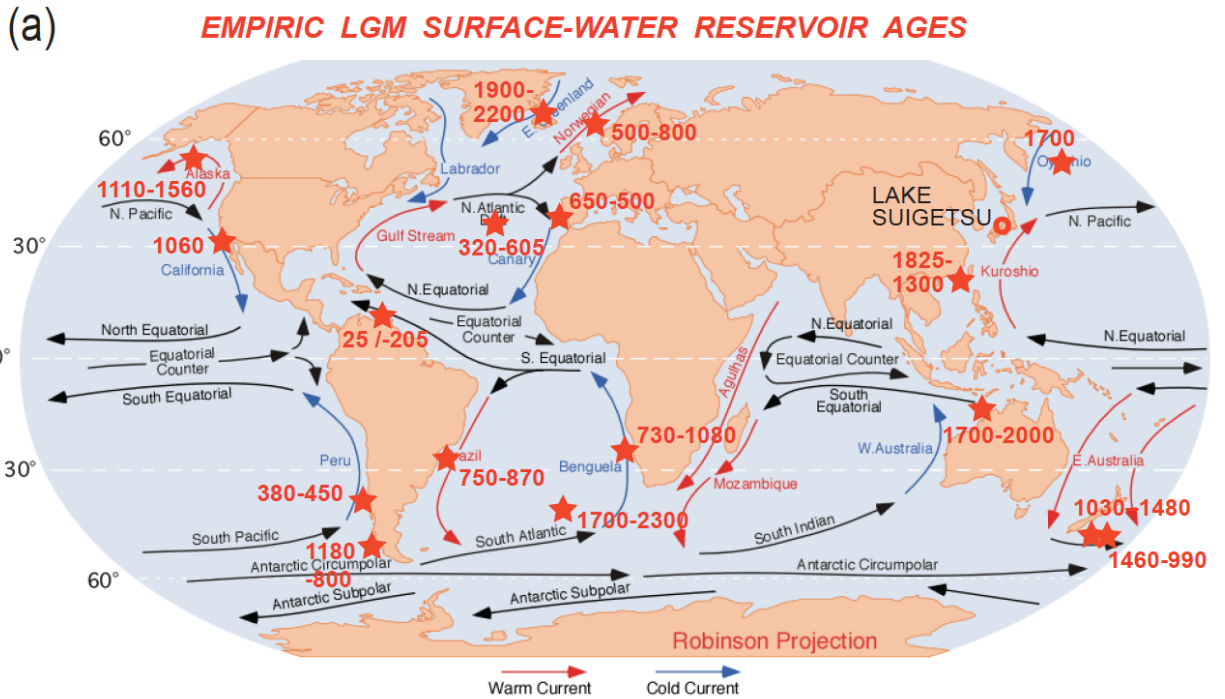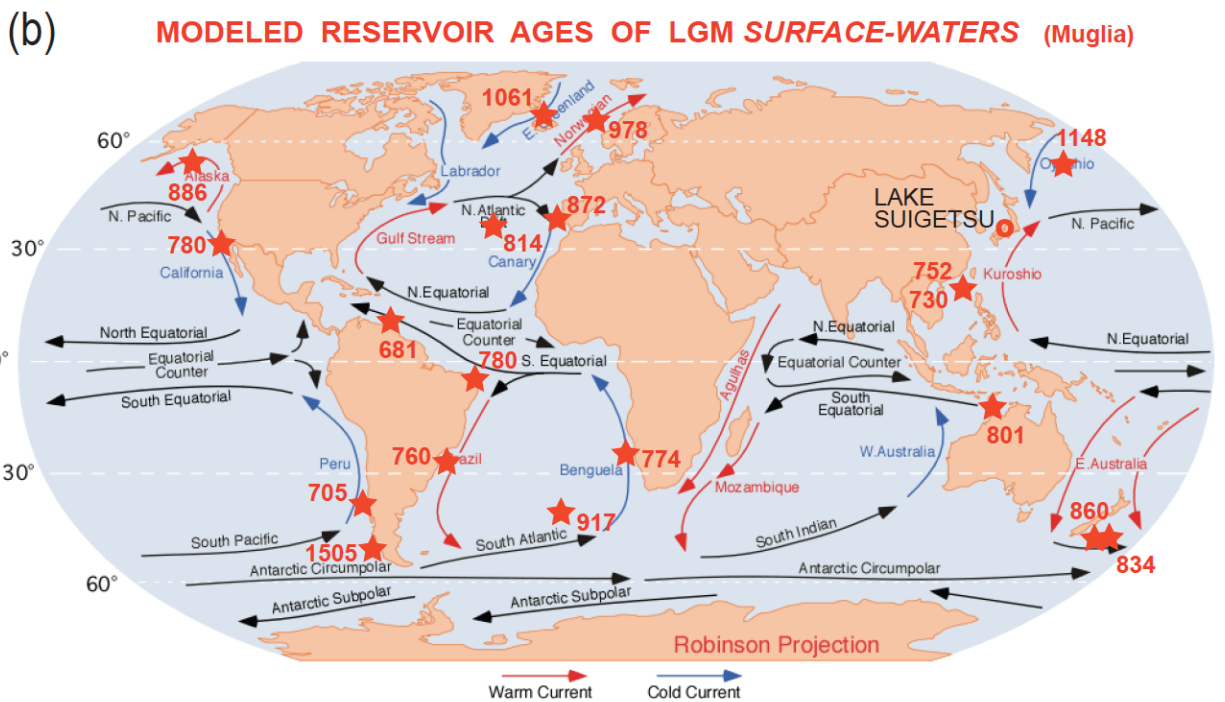
1329

1330
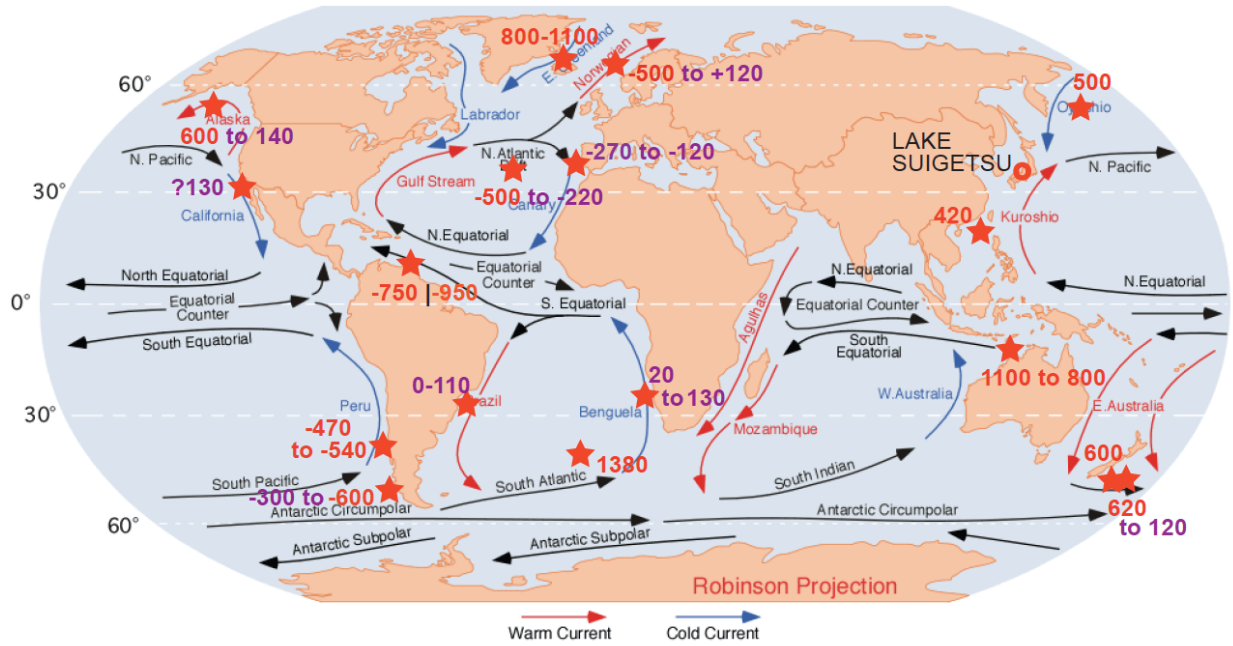
1331
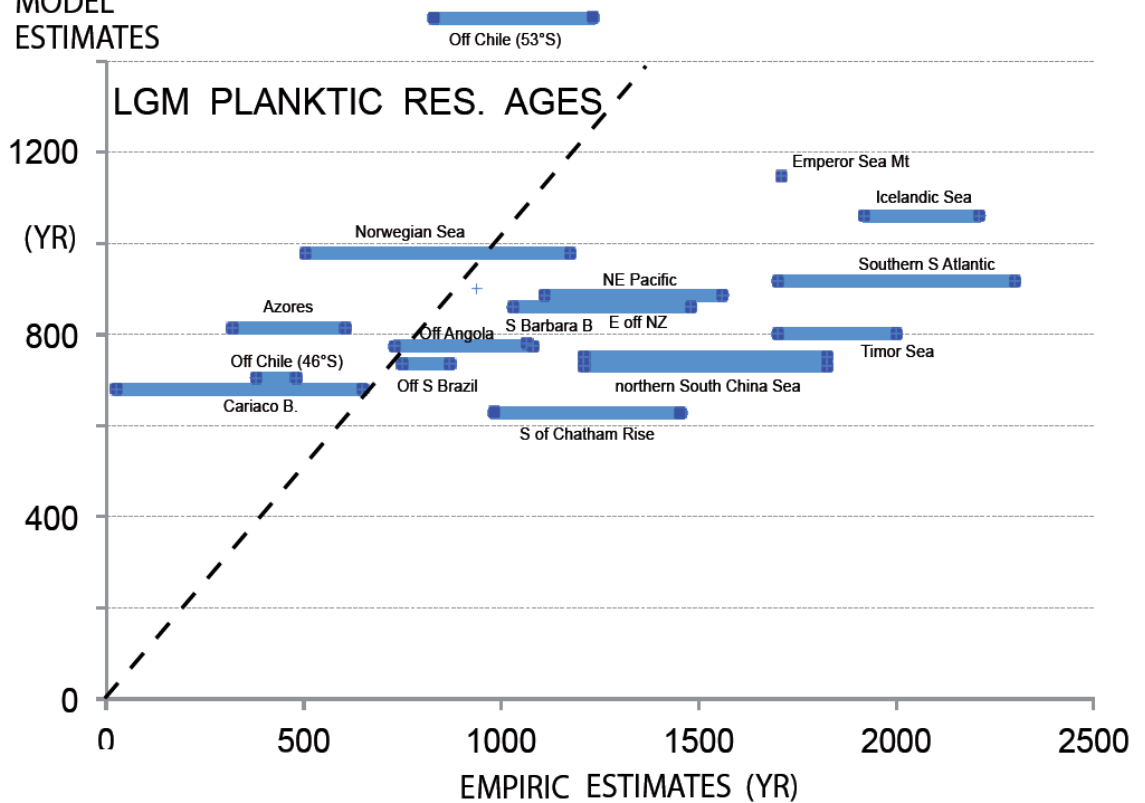
1332

1333

1334 ∀ Fig. 9. SW–NE transect of ^{14}C reservoir age and changes in ventilation age across

1335 sites GIK17940 and SO50-37 in the South China Sea during late LGM ([14]C Plateaus 5

1336 and 4; upper panel) and HS-1 (lower panel). Insert map shows location of transect and

1337 core locations. Core locations are given in Fig. 7. An extreme epibenthic δ^{13}C minimum

1338 in far southwest (Core GIK17964; Sarnthein et al., 1999) reflects an LGM incursion of

1339 Lower/Upper Pacific Deep Waters (L./ U. PAC DW) with extremely high ^{14}C ventilation

1340 age and DIC enrichment in contrast to a low ventilation age of North Pacific Deep Water

1341 (N. PAC DW). Arrows show direction of potential deep and intermediate-water currents.
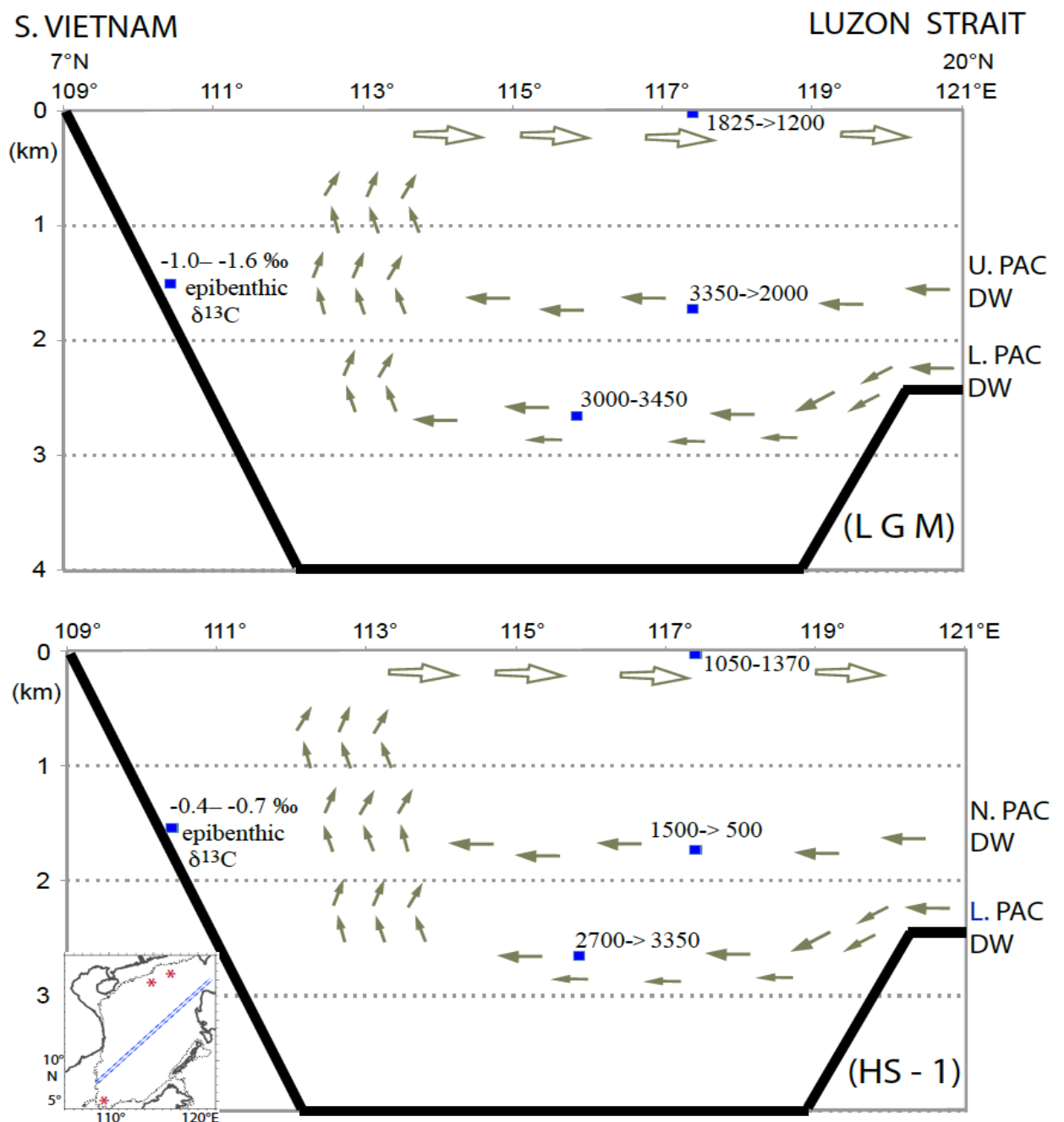
1342

1343 ⩔ Fig. 10. 2D transects of the geometries of global ocean MOC. Arrows (blue = high,

1344 yellow = poor ventilation) suggest average deep and intermediate-water currents that

1345 follow the gradient from low to high benthic ventilation ages based on paired planktic

1346 ^{14}C reservoir ages derived by means of ^{14}C plateau tuning technique (Sarnthein et al.,

1347 2013, Balmer et al., 2018, Küssner et al., 2020 subm.). At some Pacific sites reservoir

1348 ages are based on paired ^{14}C ages of planktic foraminifera and wood chunks (marked

1349 by green 'w'; Sarnthein et al., 2015; Zhao and Keigwin, 2018, Rafter et al., 2018). Red

1350 arrows suggest poleward warm surface water currents. Zigzag lines indicate major

1351 frontal systems separating counter rotating ocean currents (e.g., W of Portugal and N of

1352 MD07-307; after Skinner et al., 2014). (a) Late LGM circulation geometry (21–18.7 cal.

1353 ka), largely similar to today. Note the major east-west gradient of ventilation ages in the

1354 central North Atlantic, between Portugal (PORT) and Mid-Atlantic Ridge W of Azores

1355 (MAR). (b) HS-1 benthic ventilation ages reveal a short-lasting MOC reversal leading to

1356 Atlantic-style overturning in the subpolar North Pacific and coeval Pacific-style stratific-

1357 ation in the northern North Atlantic, with seesaw-style reversals of global MOC at the

1358 onset and end of early HS-1 (first proposed by Broecker et al., 1985, however, for LGM

1359 times). Increased ventilation ages reflect enhanced uptake of dissolved carbon in the

1360 LGM deep ocean (Sarnthein et al., 2013), major drops suggest major degassing of CO_2

1361 from both the deep Southern Ocean and North Pacific during early HS-1. – SCS =

1362 South China Sea. AABW = Antarctic Bottom Water; AAIW = Antarctic Intermediate

1363 Water. NADW = North Atlantic Deep Water. Small arrows within age numbers reflect

1364 temporal trends. Many arrows are speculative using circumstantial evidence of benthic

1365 δ^{13}C records and local Coriolis forcing at high-latitude sites per analogy to modern

1366 scenarios. Location of sediment cores are given in Fig. 7, short-term variations in

1367 planktic and benthic ^{14}C reservoir/ventilation age in Suppl. Fig. S2 and Table 3.

1368
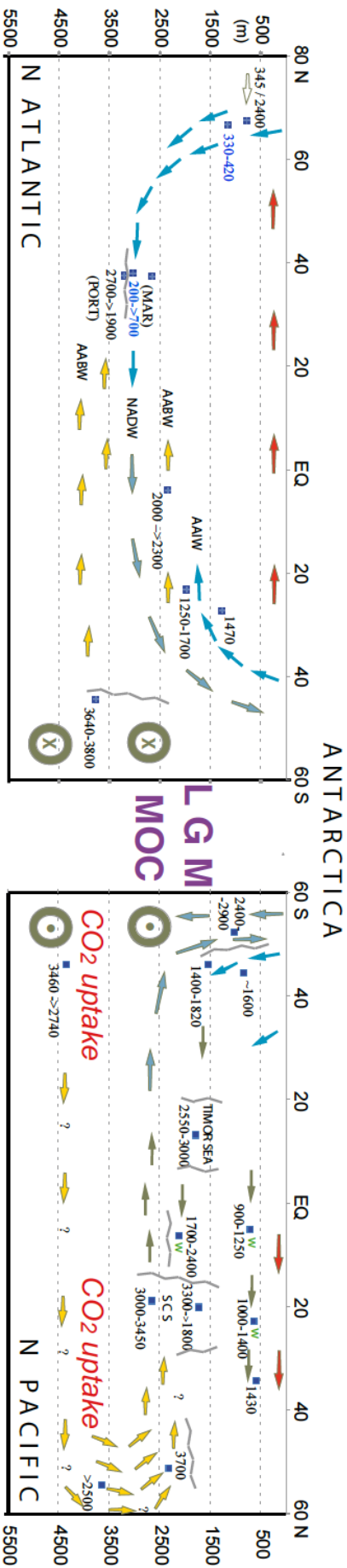
1369

1370 ⊻ Fig. 11. Global distribution of ¹⁴C reservoir ages obtained (a) for late LGM

1371 intermediate waters (100–1800 m w.d.) and (b) for LGM deep waters (>1800 m w.d.,

1372 including Site GIK 23074 at 1157 m in the Norwegian Sea).

1373

1374